ANNUAL REVIEWS

Annual Review of Fluid Mechanics

The Fluid Dynamics of Disease Transmission

Lydia Bourouiba

The Fluid Dynamics of Disease Transmission Laboratory, Massachusetts Institute of Technology, Cambridge, Massachusetts 02139, USA; email: lbouro@mit.edu

Annu. Rev. Fluid Mech. 2021. 53:473–508

First published as a Review in Advance on October 6, 2020

The *Annual Review of Fluid Mechanics* is online at fluid.annualreviews.org

https://doi.org/10.1146/annurev-fluid-060220-113712

Keywords

fragmentation, multiphase flows, interfacial flows, turbulence, disease transmission, pathogen footprint, COVID-19

Abstract

For an infectious disease such as the coronavirus disease 2019 (COVID-19) to spread, contact needs to be established between an infected host and a susceptible one. In a range of populations and infectious diseases, peer-to-peer contact modes involve complex interactions of a pathogen with a fluid phase, such as isolated complex fluid droplets or a multiphase cloud of droplets. This is true for exhalations including coughs or sneezes in humans and animals, bursting bubbles leading to micron-sized droplets in a range of indoor and outdoor settings, or impacting raindrops and airborne pathogens in foliar diseases transferring pathogens from water to air via splashes. Our mechanistic understanding of how pathogens actually transfer from one host or reservoir to the next remains woefully limited, with the global consequences that we are all experiencing with the ongoing COVID-19 pandemic. This review discusses the emergent area of the fluid dynamics of disease transmission. It highlights a new frontier and the rich multiscale fluid physics, from interfacial to multiphase and complex flows, that govern contact between an infected source and a susceptible target in a range of diseases.

I simply wish that, in a matter that so closely concerns the well-being of mankind, no decision shall be made without all the knowledge which a little analysis and calculation can provide.

—Daniel Bernoulli (1760), French Academy of Sciences, Paris

1. INTRODUCTION

The unfolding coronavirus disease 2019 (COVID-19) pandemic and the recent outbreaks of severe acute respiratory syndrome (SARS) (CDC 2017b), middle east respiratory syndrome (MERS) (CDC 2019), and highly pathogenic influenza such as H5N1 and H1N1, as well as rising antibiotic resistance, demonstrate that we live in a time of newly emerging and reemerging infectious diseases that affect billions worldwide (Bourouiba et al. 2010, Shrestha et al. 2011, Bourouiba 2013). The current coronavirus outbreak also vividly illustrates the spatiotemporal coupling of epidemics, with local outbreaks rapidly spiraling out of control and placing unprecedented burdens on national health-care systems and the global economy, with trillions of dollars already spent (CARES Act, Pub. L. 116-136), surpassing cost estimates of pandemic influenza (IMF/WB 2006). Additionally, the COVID-19 pandemic demonstrates the acute need for investment in science-based research in prevention, infection control, and predrug/vaccine disease management.

In the time of an outbreak, fundamental and urgent questions revolve around the mode of transmission and, hence, the strategy for containment and protection. How does severe acute respiratory syndrome coronavirus 2 (SARS-CoV-2) spread? How should health-care workers and the most vulnerable populations be protected when masks or respirators are in short supply? How and how often should hospital rooms, airplanes, cruise ships, and dormitories be decontaminated? How much of a distance should be kept between individuals when breathing, speaking, singing, coughing, or sneezing? Which masks are effective at source control? While these questions are particularly pressing in the time of a global pandemic, similar questions apply to seasonal influenza, which continues to claim around 500,000 lives per year worldwide (CDC 2017a), or tuberculosis, which kills more than one million individuals annually, remaining the leading cause of death from an infectious disease (WHO 2018). Similar prevention, epidemiology, and control questions can be asked for agricultural, waterborne, animal, or other human infectious diseases.

Infectious diseases spread through the transfer of pathogens, such as viruses (∼10–100 nm), bacteria (∼1 μm), and spores (∼1–10 μm) (see the sidebar titled Historical Vignettes). In recent years, research in infectious diseases on the small spatial scale has made pathbreaking advances toward understanding pathogen–host invasion, infectious disease pathogenesis, and host immunology. Additionally, detailed spatiotemporal data and associated models have been generated to predict epidemic spread across regions and countries at the large spatial scale (**Figure 1*a***). Nevertheless, a critical gap remains in our understanding of disease spread at the intermediate scale at which host-to-host transmission acts as the link between pathogen–host interactions and host physiology, on the one hand, and environmental factors and larger population-scale dynamics, on the other (**Figure 1*b***).

The transmission event may appear too brief and unpredictable to be governed by clear underlying mechanisms that could be leveraged for intervention. However, the transmission of pathogens from one host to the next is a necessary step in their life cycle. Thus, to persist, pathogens have to adapt to and survive this obligatory phase, which often involves their suspension in and interaction with a fluid. Hence, there is a clear opportunity and need to understand the mechanisms by which fluids shape the dispersal and transmission of pathogens and how pathogens may adapt to or even influence the transmission process to ensure their own cyclical survival (Zanin et al. 2016, Poulain & Bourouiba 2018, Ruhl et al. 2020).

HISTORICAL VIGNETTES

Daniel Bernoulli, well known for his contributions to hydrodynamics, initially studied medicine, graduating from the University of Basel in 1721 with a thesis entitled *Dissertatio physico-medica de respiratione*. He became a professor of anatomy and botany, and later of physics as well (Straub 1970). He was the first to apply concepts of probabilistic modeling to epidemics to estimate the effectiveness of variolation against smallpox and to understand the expected change in life expectancy if smallpox could be eliminated (Blower 2004). He thus was the first fluid dynamicist formally involved in epidemiology.

Until the nineteenth century, it was widely believed that infectious diseases were contracted through the inhalation of noxious vapors (termed miasma) emanating from decomposing matter. A core debate centered on the question of the nature and spontaneous generation of infectious agents (Nelson & Williams 2014). It was not until the late-nineteenth century that the concept of transmission of specific pathogenic agents gained traction. Systematic experiments by Pasteur (1861) and Koch (1876) on anthrax, tuberculosis, and cholera firmly tipped the scale toward the germ theory and the recognition that specific microorganisms cause infectious diseases. When Flügge (1897) demonstrated the presence of pathogens in exhaled droplets large enough to settle around an infected individual, so-called droplet transmission by direct contact with the ejected and infected fluid phase came to be viewed as the primary route of respiratory disease transmission until the 1930s.

The lack of a mechanistic understanding at the intermediate scale at which transmission occurs leads to debates, contradictory approaches, and ad hoc searches for solutions. For example, transmission routes of health-care-associated (nosocomial) infections remain debated, with a strong focus on surface cleaning as a mitigation strategy, largely neglecting or dismissing routes that pertain to air contamination and persistence of airborne pathogens. Similarly, in agriculture and

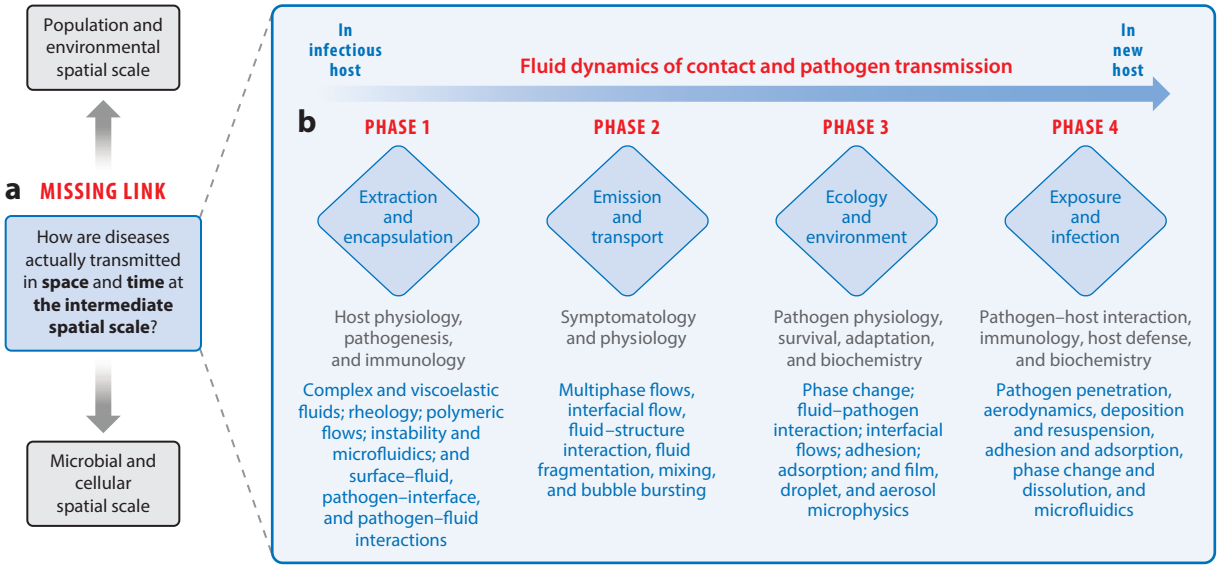

Figure 1

(*a*) Gap in knowledge of infectious disease transmission at the intermediate (host-to-host) spatial scale. (*b*) The gap is framed from the lens of the underlying physiological/biophysical (*gray*) and fluid dynamics (*blue*) processes that shape the key phases of disease transmission from an infected host to a target. The four phases establish the framework for the breakdown of transmission into tractable, mechanistic, and measurable processes.

food safety, pathogen transfer to plants or produce remains poorly characterized, leading to continued yield loss due to suboptimal prevention and control of cross contamination. Yet, it is at this intermediate scale that mechanistic understanding can lead to innovations for both nonpharmacological and pharmacological solutions, as well as strategies to control epidemics. Finally, it is at this intermediate scale that fluids are ubiquitous. Coughs or sneezes, for example, produce a high-momentum turbulent cloud of hot and moist air, propelling and dispersing pathogen-laden droplets up to 8 m in a few seconds (Bourouiba et al. 2014; Bourouiba 2016, 2020). Additionally, exhaled droplets may linger suspended in the air for hours, depending on ambient temperature and humidity conditions. Droplets can also spread from bursting bubbles (Bourouiba & Bush 2013, Walls et al. 2014, Poulain & Bourouiba 2018, Poulain et al. 2018) or splashed from a wet, contaminated surface (Lejeune et al. 2018, Poulain & Bourouiba 2018). Hence, to model and predict host-to-host infectious disease transmission, a mechanistic understanding of the underlying fluid physics is required. Following Bernoulli's wisdom in the epigraph above, to enable "a little analysis and calculation," we propose a framework to break down the complex, multifaceted transmission event into tractable, biophysically based mechanistic processes.

2. TRANSMISSION: FLUID DYNAMIC AND BIOPHYSICAL FRAMEWORK

The study of the fluid dynamics of disease transmission—or, more generally, of fluids and health—aims to elucidate the fundamental fluid dynamic and biophysical mechanisms shaping the transmission dynamics of pathogens in which drops, bubbles, and multiphase and complex flows play prominent roles in transmission processes (Gilet & Bourouiba 2014, 2015; Bourouiba et al. 2014; Bourouiba 2016, 2020; Jung et al. 2016; Scharfman et al. 2016; Wang & Bourouiba 2017, 2018a,b, 2020a,b; Lejeune et al. 2018; Poulain & Bourouiba 2018; Poulain et al. 2018; Wang et al. 2018a; Bahl et al. 2020; Jones et al. 2020; Y. Wang & L. Bourouiba, manuscripts in review). Here, "health" is defined broadly to include human, plant, and animal populations. Specifically, disease transmission in these populations involves a hierarchy of fluid dynamic and biophysical processes shaping pathogen emission, dispersal, persistence, and successful new host infiltration and infection. To develop a comprehensive understanding of the end-to-end transmission process, we must decipher the underlying physics of these processes, and in particular the rich multiscale and multiphase fluid dynamics involved and its interaction with the pathogen. We propose a framework based on these distinct physical phases driving transmission and contact (**Figure 1**):

- Phase 1: in-host extraction and encapsulation of pathogens;
- Phase 2: emission from host and transport of pathogens;
- Phase 3: ecology and persistence of pathogens in the environment; and
- Phase 4: new-host infiltration and infection.

In this review, we illustrate this framework in the context of respiratory and nosocomial diseases (Sections 3 and 4), water-to-air pathogen transfer (Section 5), and pathogen transmission in agriculture (Section 6). We conclude by reviewing current work in unsteady fluid fragmentation (Section 7) at the core of the transmission dynamics in these application domains (**Figure 2**) before closing with a summary of the current gaps in our understanding and opportunities for future research at this exciting and critically important emerging domain of fluids and health (Section 8).

3. RESPIRATORY PATHOGEN TRANSMISSION

The current COVID-19 pandemic has led to unprecedented containment policies throughout the world in an effort to stem the spread of the SARS-CoV-2 virus. Since the first reports of

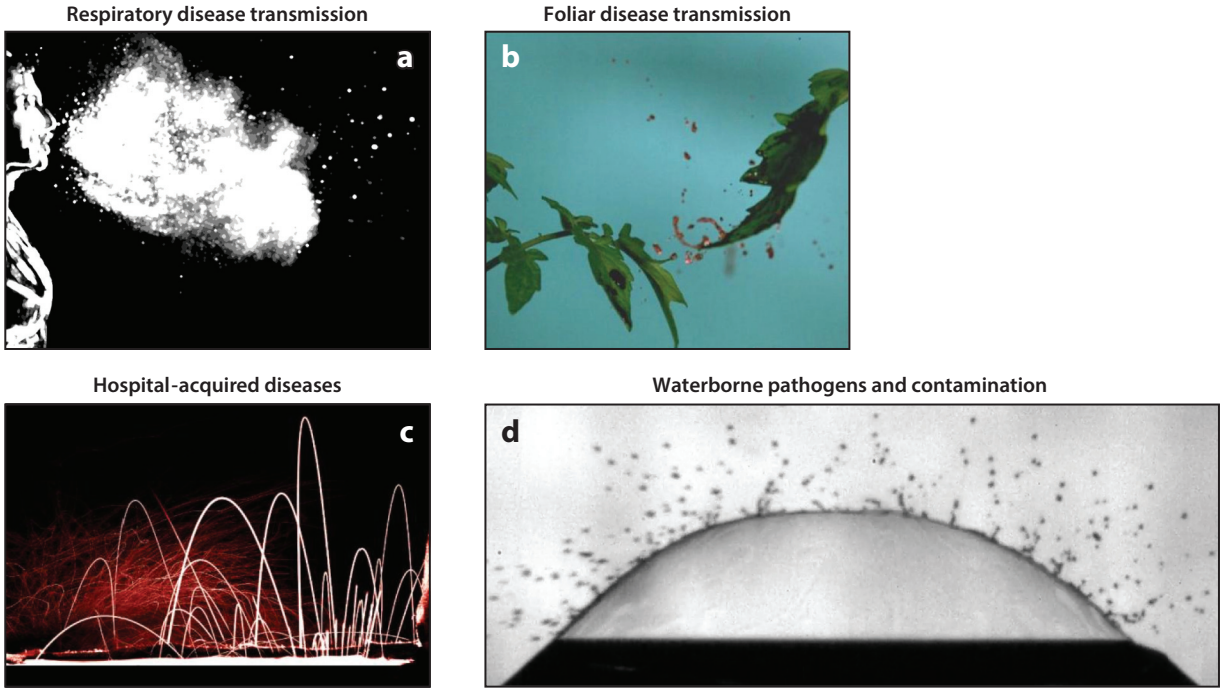

Figure 2

Examples of fluid dynamic processes involved in (*a*) pathogen transfer in respiratory disease transmission (turbulent gas cloud emission), (*b*) foliar disease transmission (drop-on-leaf fluid–structure interaction), (*c*) health-care-associated contamination (complex fragmentation), and (*d*) waterborne disease transmission (bubbles and interface destabilization, e.g., bubble bursting). Photographs reprinted with permission from (*a*) Bourouiba (2016), copyright 2016 Massachusetts Medical Society; (*b*) Gilet & Bourouiba (2015), copyright 2015 the authors; (*c*) Traverso et al. (2013), copyright 2013 the authors; and (*d*) Poulain & Bourouiba (2018), copyright 2018 American Physical Society.

an infectious disease outbreak in the Chinese province of Hubei, public health officials sought to understand how this new virus spreads. Even as of July 2020, the transmission mechanism of SARS-CoV-2 remains debated (Bourouiba 2020, Lewis 2020). Furthermore, the transmission mechanisms of even the most common respiratory diseases remain poorly understood. Here, we focus on the fluid dynamics of exhalations as vehicles of respiratory pathogen transmission. Exhalations, including breathing out, talking, laughing, coughing, sneezing, and singing (Duguid 1945, Bourouiba et al. 2014, Hamner et al. 2020), fall into Phase 2 of the transmission framework (**Figure 1**). We now know that they all involve the emission of a gas phase laden with droplets of a range of sizes. The momentum, total volume, and liquid volume fraction of these emissions determine their spatiotemporal probability density function of contamination in the air and on surfaces—what we term the "pathogen footprint."

3.1. From Isolated Droplets to Multiphase Clouds as Vehicles of Pathogen Spread

Throughout the early twentieth century, it remained a common belief that most respiratory infectious diseases spread via direct contact with macroscopically visible droplets emitted by an infected individual (see the sidebar titled Historical Vignettes). This view prevailed until the 1930s when William Wells investigated tuberculosis transmission (Wells 1934, 1955).

DROPLETS, DROPLET NUCLEI, AEROSOLS, AND AIRBORNE TRANSMISSION

The terminology in pathogen transmission has been coined by different disciplines and hence is subject to different meanings in different disciplines. For the purposes of this review, we consider a "droplet" as liquid fluid and "droplet nuclei" as the solid residues remaining after liquid droplet desiccation has taken place to leave in place solid complex residual material. Respiratory droplets, for example, range in size from $\mathcal{O}(1\ \mu m)$ to $\mathcal{O}(1\ mm)$, while a droplet residue/nucleus is estimated to be smaller than $\sim 10\ \mu m$ depending on the initial size and composition. Both droplets and droplet nuclei can remain suspended in the air, and hence can be airborne vehicles of pathogen transmission. This definition is in contrast to the term "aerosol," which is an umbrella term for any type of matter suspended in the air (Hirst 1995). Adding to the confusion, airborne transmission in infectious disease control is defined as "dissemination of either airborne droplet nuclei or small particles in the respirable size range containing infectious agents," seemingly excluding droplets from the definition (Siegel et al. 2007). It would seem prudent, particularly in the time of an ongoing global pandemic, for the different communities to settle on a single, unambiguous, and universally accepted definition to avoid confusion in the scientific literature, the popular press, and public health policy (Khamsi 2020). Here, the terminology we propose is to set a universal definition based on clear physical composition. After all, no dry nuclei or residues are ever emitted from an infected host. Only droplets—liquid—of various sizes are emitted; they then evolve to evaporate into residues or nuclei at various rates and in different manners depending on the physics of their emission and composition and the characteristics of the ambient air.

For droplets ranging in diameter from 1 to 1,000 μm, Wells compared the time for complete evaporation of isolated droplets to their settling time and reported that drops with diameter $d > 100\ \mu m$ settle in liquid form to the ground in less than one second. Drops with $d < 100\ \mu m$ typically evaporate and become droplet nuclei that remain suspended in the air (Wells 1934, 1955). Hence, a physics-based dichotomy was born that classified respiratory transmission into the large- versus small-droplet routes or, alternatively, between droplets versus aerosols, on the basis of initial droplet diameter. The implications of Wells's results are that large droplets settle within the immediate vicinity of an exhaling individual while small droplets evaporate, forming airborne droplet nuclei (see the sidebar titled Droplets, Droplet Nuclei, Aerosols, and Airborne Transmission). Wells encountered major criticism by and resistance from the medical community (Hare 1964) although, with the supporting evidence from a series of systematic and careful experiments, this dichotomy was eventually accepted.

A fluid dynamic analysis of this picture reveals that isolated visible droplets follow ballistic trajectories and, depending on their initial momentum, may settle within 1 to 2 m of a sneezing or coughing subject, as seen with the naked eye in experiments by Flügge (1897) and many others in the late nineteenth and early twentieth centuries. However, isolated droplets typically below 100 μm in diameter encounter significant drag from the ambient air, reducing their range even if they were emitted with speeds as high as 100 m/s. Hence, in the physical picture derived from Wells's work, larger droplets are thought to travel farther than smaller droplets, and the dichotomy between large versus small routes cannot lead to contamination distances larger than about 2 m in quiescent/still ambient air. Only ambient airflow may extend the range of droplet nuclei through advection, typically on the order of centimeters per second indoors. Hence, the maximum distances reached by these droplet nuclei would not be inherent to the exhalation emission dynamics of speaking, coughing, or sneezing, but would be completely determined by localized weak advective flows of ventilation and climate control systems in indoor environments.

This large-versus-small droplet dichotomy remains at the core of the World Health Organization (WHO) and Centers for Disease Control and Prevention (CDC) classification schemes still

DROPLET SIZE DISTRIBUTIONS AND THEIR MEASUREMENTS

The wide range of experimental techniques in use to determine droplet size distributions has led to conflicting results (e.g., Duguid 1946, Yang et al. 2007, Morawska et al. 2009, Papineni & Rosenthal 2009, Johnson et al. 2011, Zayas et al. 2012). Techniques range from droplet enumeration on glass slides to optical counting, aerodynamic droplet sizing, interferometric Mie imaging, droplet image velocimetry, electric low-pressure impactor spectrometry, scanning mobility droplet sizing, and laser diffraction. A range of instrumentations and calibrations are associated with these techniques, typically requiring a priori assumptions about optical properties of the droplets or particles and their evaporation rates, shapes, sphericity, and compactness. These properties are particularly difficult to infer for droplets made of complex biological fluids or materials, making these measurements highly variable. They have varying sensitivities across the size spectrum, are not necessarily calibrated to a common reference range, and tend to only sample a small volume, which can amplify background noise (Alsved et al. 2020). Additionally, droplet sizes often tend to be determined only at a single sampling location (typically away from the source) and are highly sensitive to ambient conditions (humidity and temperature). This poses a basic undersampling problem in space and time that is particularly acute for resolving highly transient, unsteady emissions. Finally, in addition to the droplet sizes, one ideally wishes to determine whether pathogens are present and remain infective or live in the droplets as a function of droplet size. This determination depends on the droplet volume sampled, handling procedures, and amplification approaches (Ouyang & Han 2019, Mbareche et al. 2019). A mechanistic understanding of the relevant fluid fragmentation processes generating the droplet sizes and speeds is complementary to the refinement of measurement techniques by providing physically based expected bounds and physical constraints on the range of droplet size and speed distributions for physiological fluids.

used and debated today in the context of COVID-19, just as it was for SARS. Various arbitrary-diameter cutoffs, from 5 to 10 μm, are used to classify host-to-host transmission in respiratory infectious diseases. Not surprisingly, researchers became very interested in the size distribution of exhaled droplets as a function of exhalation type, such as breathing, speaking, coughing, and sneezing (see the sidebar titled Droplet Size Distributions and Their Measurements). Accordingly, determining whether a pathogen spreads primarily via the droplet or the aerosol route becomes a major focus for infection control specialists each time a new respiratory infectious disease emerges (Boseley 2020). As explained below, two problems immediately arise with this approach, both of which call for abandoning the false droplet-versus-aerosol transmission dichotomy.

The first problem is that public health agencies mostly try to infer dominant routes of transmission from large-scale population epidemic data, subject to all the limitations, sparsity, and underreporting inherent to such data (Atkins et al. 2015). Clusters of infected acute cases in a household could result either from the large- or small-droplet route or through direct contact with contaminated shared surfaces. Inherently, the data at the (large-scale) epidemic or case-clustering epidemiologic level cannot distinguish between the routes of transmission. Only studies at the intermediate (host-to-host) scale can elucidate and quantify the prevailing transmission mechanisms and so reveal the governing rules, shaped by the coupled physics and biology of transmission (**Figure 1*b***). Coupled to this methodology issue is the common misconception that the airborne route of transmission implies highly effective long-range transmission at the scale of entire buildings or cities and that the lack of such explosive transmission patterns necessarily implies transmission by large droplets only.

The second problem is that exhalations do not emit isolated droplets that either evaporate and contaminate the air or settle to the ground and contaminate surfaces in the immediate vicinity of the subject. Exhalations release a multiphase fully turbulent puff cloud that is composed of

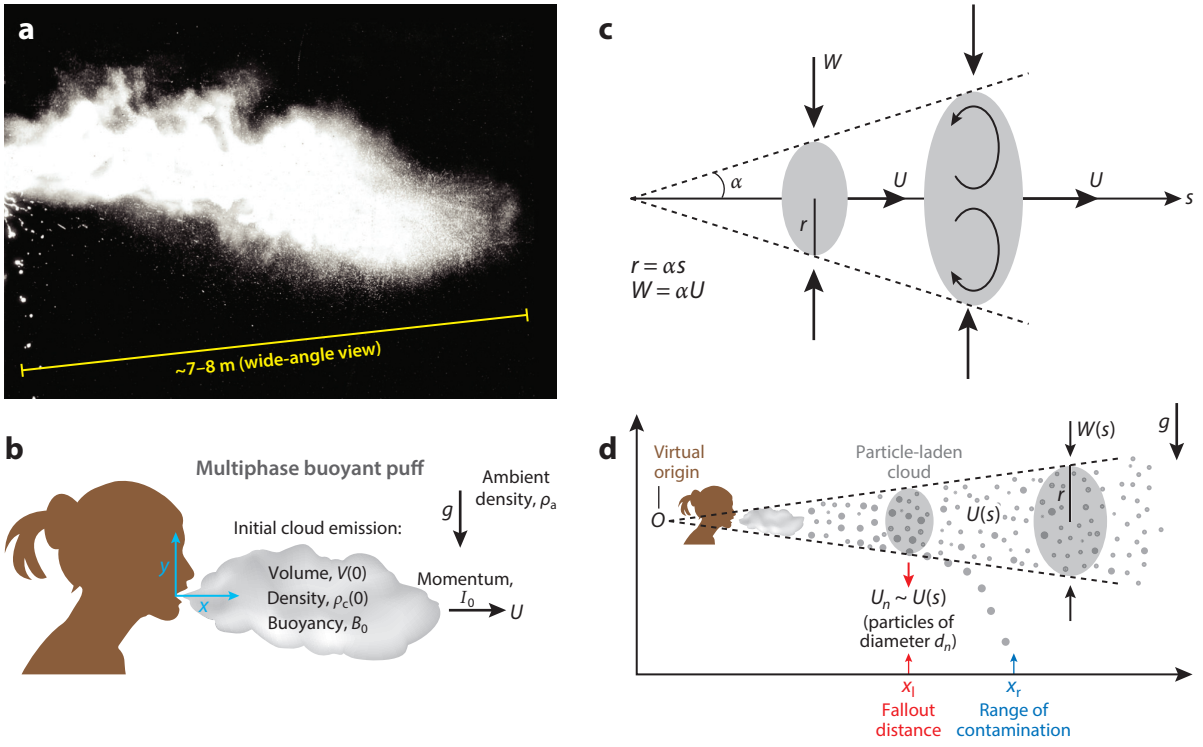

Figure 3

(*a*) Exhalations such as breathing, coughing, and sneezing release a turbulent puff cloud of hot and moist air containing suspended droplets trapped within it. The cloud and its payload can travel up to 8 m in the case of sneezes, for example (Bourouiba 2020). (*b*) The initial cloud emission is described by a volume $V(0)$, density $\rho_c(0)$, initial buoyancy B_0, and momentum I_0. (*c*) As the cloud moves forward along its trajectory $s(t)$, and with average cross-sectional velocity $U(t)$, it entrains ambient air with average speed $W(t) = \alpha U(t)$ and cloud radius $r(t) = \alpha s(t)$, where α is a (constant) entrainment coefficient. The fully turbulent flow is self-similar along its trajectory away from a point source. (*d*) Negatively buoyant suspended droplets circulate within the cloud until they settle out (at horizontal distance x_f) and reach a final position x_r, setting the contamination range of droplets of a given size (Bourouiba et al. 2014). Depending on the ambient environmental conditions, the cloud may also rise as it moves forward if it is sufficiently buoyant, possibly entering ventilation systems with its residual payload. Panels adapted with permission from (*a*), Bourouiba (2020), copyright 2020 American Medical Association; and (*b–d*) Bourouiba et al. (2014), copyright 2014 Cambridge University Press.

warm and moist exhaled air and suspended mucosalivary droplets of a full range of droplet sizes, ranging from $\mathcal{O}(1\ \mu m)$ to $\mathcal{O}(1\ mm)$ (**Figure 3*a*,*b***) (Bourouiba et al. 2014; Bourouiba 2016, 2020). Throughout the cloud's evolution, droplets of all sizes settle out continuously to contaminate surfaces, while smaller droplets evaporate and turn into droplet nuclei. This distinction between the dichotomized, static view of Wells and the continuous cloud evolution view is not merely academic. Indeed, the emitted gas cloud extends the range of droplets of all sizes by trapping them and carrying them forward farther than they would reach had they been emitted as isolated droplets in quiescent air. In addition to the cloud momentum and its ability to extend the range of the droplets of all sizes within it, the locally moist exhaled gas can protect the droplets against evaporation in the typically drier and colder ambient atmosphere (compared to the warm and fully humidified conditions within the respiratory system) (Bourouiba 2020). Hence, the fluid dynamics of the exhaled multiphase turbulent puff cloud has significant real-life implications for determination of safety and physical/social distancing, respiratory protection needs for

health-care workers, and indoor air hygiene solutions (Bahl et al. 2020, Bourouiba 2020, Jones et al. 2020), which are all pressing needs that public health policy makers are forced to formulate on the go today for COVID-19 due to the lack of investments in these areas of research over past decades.

Reynolds number: inertia force divided by the viscous force, with average value $Re = Q/\nu d_m$ or $u' d_m/\nu$

3.2. Modeling the Turbulent Multiphase Exhalation Gas Cloud

Puffs, jets, thermals, and plumes are turbulent bodies of fluid ejected from a point source either continuously (in the case of plumes and jets) or discontinuously (in the case of puffs and thermals). Thermals and plumes are buoyancy driven, while puffs and jets are momentum driven (Scorer 1978, Turner 1979).[1] Their lateral extent increases linearly with distance from the source due to lateral momentum diffusion and as edge eddies entrain ambient air. The observation of self-similarity for these turbulent flows is captured by the entrainment hypothesis (Morton et al. 1956), enabling closure of the governing equations and ensuring analytical tractability.

Taking the average velocity at a given point along the trajectory, the mean lateral speed W of the ambient fluid drawn into the cloud is proportional to the mean forward cloud speed along its trajectory, U. Similarly, the cloud radius r increases linearly with the distance s from the source: $W(s) = \alpha U(s)$ and $r(t) = \alpha s(t)$ (Morton et al. 1956) (**Figure 3*c***). The entrainment coefficient α is constant, although it can differ for different types of flows (thermal, plume, puff, or jet). This turbulent point-source theory captures key features at various scales of geophysical and environmental flows (e.g., Scorer 1978, Gonnermann & Manga 2007, Woods 2010). The entrainment hypothesis has also been leveraged to mechanistically and quantitatively describe the dynamics of violent exhalation events (Bourouiba et al. 2014). The fate of the suspended droplets can be determined by drawing an analogy with multiphase particle-laden clouds that arise in a variety of geophysical systems, such as riverine outflows or industrial waste discharges (e.g., Scorer 1978, Socolofsky et al. 2002, Bush et al. 2003, Hunt et al. 2007).

In the context of exhalations, the point source is the mouth whose diameter ($d_m \sim 2$ cm) is small compared to the distance of evolution of the cloud, which is on the order of meters. The average Reynolds number (Re), estimated with the volume rate, Q (m^3/s), the kinematic viscosity ν (m^2/s), and the diameter d_m, is $Re \sim \mathcal{O}(10^4)$ for coughs and sneezes—well into the turbulent regime. The instantaneous Re can be even higher when considering the peak instantaneous velocities in the cloud. There are two phases of cloud evolution that are of relevance. The first (ejection) phase is dominated by a brief jet-like dynamics—a high-momentum release of the exhaled gas cloud and its mucosalivary payload. Let $s(t)$ be the trajectory of the jet's centroid and $r(t)$ the radius orthogonal to $s(t)$. The conservation of momentum flux, $M_0 \sim \rho r^2 (ds/dt)^2$, of the jet combined with the self-similar growth of the cloud, $r \sim s$, leads to $ds/dt \sim 1/s$ and, hence, $s \sim t^{1/2}$. The second (evolution) phase of the cloud has a longer-lasting puff dynamics that is characterized by the previously mentioned self-similar growth of the puff cloud, $r \sim s$, and conservation of momentum (in the absence of buoyancy), $I_0 \sim \rho r^3 (ds/dt)$. Thus, we have $ds/dt \sim 1/s^3$ and $s \sim t^{1/4}$. These predictions were experimentally validated in coughs and sneezes and in physical analog experiments capturing the regimes of cough and sneeze emissions (Bourouiba et al. 2014).

[1] Note that vortex rings, like puffs, are discrete emissions of momentum, which is conserved along the ring's trajectory. However, vortex rings are laminar rather than turbulent, and hence have a distinct entrainment mechanism of ambient flow and temporal evolution (Maxworthy 1972). As they proceed from the point source, the multiscale turbulent emissions remain self-similar, spanning a conical shape along their trajectory (**Figure 3*c***).

While exhalation clouds are initially driven by momentum, they can have varying degrees of initial buoyancy, as they are generally warmer and more humid than common ambient environments. In a nonstratified ambient, which is typically the case in regular-ceiling-height indoor environments with mixing ventilation (Linden 1999), it can be shown that such buoyancy is conserved. Although initially negligible, such buoyancy can ultimately influence the cloud trajectory once the forward velocity has sufficiently slowed down (Bourouiba et al. 2014). Hence, at first order, one can model the cloud as a multiphase turbulent puff with initial momentum I_0 and initial buoyancy B_0 that depends on the composition of the mixture and ambient conditions. One may choose to also resolve the initial short jet phase, which lasts on the order of 100 ms, depending on the emission type and question of interest: very short-range exhalation in a mask on the order of 30 cm versus room contamination on the order of meters.

Bourouiba et al. (2014) modeled the multiphase cloud with initial density $\rho_c(0) = \sum_{n=1}^{N}(\rho_p - \rho_f)\phi_n(0) + \rho_f$, where ρ_p is the density of the droplets and ρ_f is the density of the gas phase. The term $\phi_n(0)$ is the initial volume fraction of the suspended droplets of diameter d_n, i.e., $N_n v_n/V(t)$, where $v_n = \pi d_n^3/6$ is the drop volume, $V(t)$ is the cloud volume, and N_n is the number of drops of diameter d_n suspended in the cloud. The cloud moves forward, entraining ambient fluid of density ρ_a and assuming a volume $V(t) = V(0) + V_a(t)$, provided that the drops remain suspended in the cloud. As the drops in fact continuously settle out from the cloud, the volume change must also account for that loss with an additional term. The volume fraction of the liquid phase in real coughs and sneezes is $\mathcal{O}(10^{-6}$–$10^{-5})$ (Duguid 1946), hence small enough ($\ll 1\%$) to neglect modifications to droplet speed via collective or coalescence effects. The cloud density evolves according to

$$\rho_c(t) = \frac{V(0)}{V(t)}(\rho_f - \rho_a) + \rho_a + \sum_{n=1}^{N}\phi_n(t)(\rho_p - \rho_f), \qquad 1.$$

where the volume fraction of suspended drops of diameter d_n at time t is $\phi_n(t) = N_n(t)v_n/V(t)$, and all suspended drops have the same density, ρ_p (Bourouiba et al. 2014).

Within this framework, droplets remain suspended within the puff until their settling speed U_n (obtained from balance of drag and weight for drops of diameter d_n) becomes comparable and exceeds the mean circulation speed within the puff, $U_n \sim U(s)$. As the puff speed necessarily decreases with distance from the source due to momentum conservation, so does the size of the suspended drops: Drops and droplet nuclei with settling speeds that are much smaller than the average overturning speed of the cloud over all of its trajectory remain suspended within the puff for a significant distance, $\mathcal{O}(10$ m). Once the cloud's speed is close to null, these drops and nuclei may then be advected by background ventilation flows on the order of centimeters per second, possibly for hours to days until they adhere on surfaces or are successfully extracted by indoor ventilation air-change cycles.

Martin & Nokes (1988) proposed an elegant model to describe particle settling from a turbulent fluid in a bounded container. They assume that the fluid is well mixed and turbulent and that the particle settling speed, U_n, is negligible compared to the characteristic turbulent speed. The particles thus remain mostly suspended with a continuous settling into the lower boundary layer over a timescale $\sim h/U_n$, where h is the height of the container. Following such ideas, Bourouiba et al. (2014) developed a model of continuous particle fallout from the exhalation cloud in which particles settle out continuously from the cloud's edge prior to final fallout: $U_n \sim U(s)$ (**Figure 3*d***). Assuming that the droplets are homogeneously mixed within the cloud, the continuous fallout governs the number $N_n(t)$ of droplets of size d_n within the cloud:

$$\frac{dN_n}{dt} = -\frac{3U_n N_n(t)}{2\alpha s(t)}. \qquad 2.$$

The continuous fallout model has been validated, with good agreement with analog experiments (Bourouiba et al. 2014). The resultant theoretical model is closed: It does not contain free parameters. It can be used to provide the spatiotemporal evolution of the gaseous cloud in normal exhalations, coughs, and sneezes, along with the number and volume of droplets falling out of the cloud as a function of time and distance from the source. This is at the core of the computation of the pathogen footprint and, hence, of risk map analyses of contamination (Bourouiba et al. 2014, Bourouiba 2016).

The predicted cloud evolution was validated against analog laboratory and human-subject experiments (Bourouiba 2020). It demonstrates the importance of the gas phase and its momentum by (*a*) extending the range of its droplet payload by more than a factor of 200, reaching up to 7–8 m for sneezes, for example; and (*b*) determining that the droplets that reach the farthest and fastest are the smallest ones, even without any background airflow. Hence, the dichotomized transmission view as inspired by Wells in the 1930s, which inherently ignores the presence of an exhaled multiphase gas cloud, is not adequate to predict the range of surface and air contamination resulting from exhalations, requiring a fundamental paradigm shift (**Figure 4**). Moving away from the isolated drop emission view to the turbulent, multiphase puff cloud model enables transmission to be reframed in terms of air versus surface contamination levels in space and time (the pathogen footprint) when evaluating the risk and efficacy of interventions pertaining to indoor space management and occupancy.

Finally, as discussed earlier, all exhalations—breathing out, sneezing, coughing, talking, and singing—have the same physical description of a point-source emission of a turbulent (high-Re), multiphase gas cloud laden with respiratory liquid droplets and where the momentum driving the motion is in the gas phase rather than the liquid droplet phase (or spray). The only distinctions between these various emissions include the air volume emitted (∼500 mL for regular exhalations and 1–4 L for coughs and sneezes), the momentum as modulated by the duration of emission (∼2 s for a tidal breathing, ∼200–300 ms for a cough, and ∼100–200 ms for a sneeze), the liquid volume fraction, the droplet size distribution and composition, and the frequency of these respiratory events (∼12 breaths per minute for regular exhalations and 5–30 coughs or sneezes per hour, depending on symptomatology). With $Re \sim \mathcal{O}(10^4)$ for coughs and sneezes and $\mathcal{O}(10^3)$ for breathing, these exhalations are all in the turbulent gas phase regime, reaching different ranges, in order of decreasing momentum: sneezing, coughing, singing, talking, and normal (tidal) breathing.

3.3. Unsteady Fragmentation of Mucosalivary Fluids

Droplet formation is a complex process, as the mucosalivary fluid is either ejected in already formed droplets or formed in the respiratory tract through a combination of shear and film rupture instabilities or in the form of sheets that are stretched and rupture into rings and fluid ligaments, which ultimately destabilize into droplets entrapped in the turbulent gas phase (**Figure 5**) (Scharfman et al. 2016). Such destabilizations, which can be governed by combinations of, for example, versions of Kelvin–Helmholtz, Rayleigh–Plateau, and Rayleigh–Taylor instabilities, involve surface tension and viscous and aerodynamic forces (Eggers & Villermaux 2008), the relative magnitudes of which determine the regimes of fragmentation and final droplet size and speed distributions found within the exhaled turbulent puff cloud. Higher surface tension and fluid viscosity generally favor the formation of larger droplets, while higher air speeds tend to favor the generation of smaller droplets.

The fragmentation processes involved in the breakup of muscosalivary fluid are inherently unsteady (Scharfman et al. 2016, Wang et al. 2018a) and hence are not well described within the established theoretical framework of steady fluid fragmentation. Furthermore, the liquid phase of

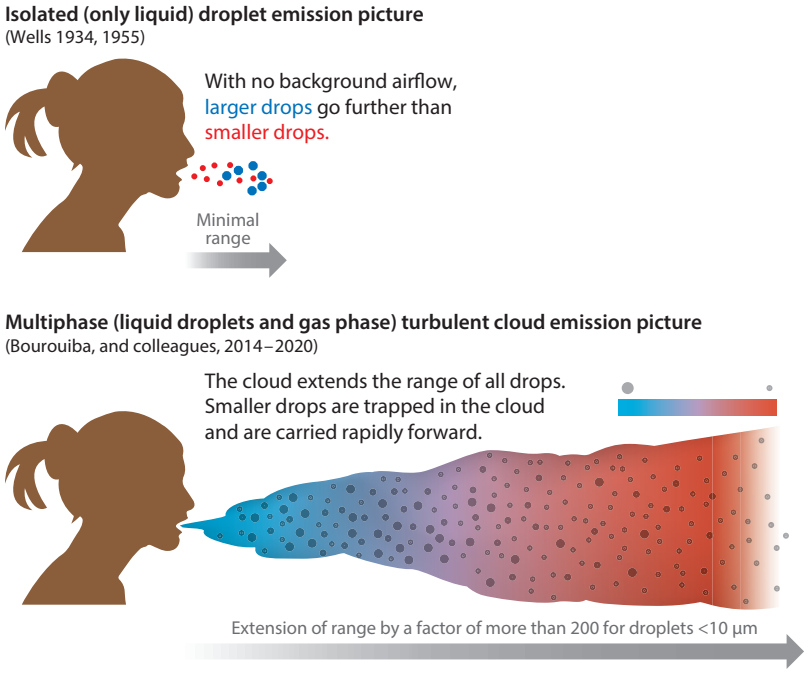

Figure 4

Contrasting the isolated droplet emission picture of Wells (1934, 1955) with the recently developed turbulent gas cloud emission picture of exhalations (Bourouiba et al. 2014; Bourouiba 2016, 2020). (*Top*) In the isolated droplet picture, larger droplets follow ballistic trajectories, settling within 2 m of an exhaling, speaking, coughing, or sneezing subject, while smaller droplets remain closer, encountering significant drag. Hence, without background airflow, larger droplets travel farther than smaller droplets and the resulting droplet nuclei. Thus, the range of contamination is set by the larger droplets. (*Bottom*) However, respiratory droplets are not in fact emitted as isolated droplets but are trapped in a turbulent gas cloud that extends the range of droplets of all sizes, with a continuous partial settling of all sizes and retention of drops and nuclei of settling speeds smaller than that of the cloud. Thus, smaller droplets and nuclei travel quickly with the cloud (on the order of seconds) the farthest (on the order of meters), even without background airflow.

Deborah number: ratio of extensional relaxation and capillary timescales; $De = \lambda/\tau$

Ohnesorge number: relative magnitude of viscous to inertial and surface tension forces; $Oh = \mu/\sqrt{\rho\sigma d} = \sqrt{We}/Re$

Weber number: ratio of kinetic to surface energy; $We = \rho u^2 d/\sigma$

interest for this problem is a complex mixture of saliva and mucus, the relative fraction of which is a function of the location of generation within the respiratory tract. While mucosalivary fluid is mostly composed of water (97%), it contains other components, such as salts, proteins, and fatty acids (Bansil & Turner 2006), as well as dissolved large glycoprotein mucins and other biopolymers that give rise to its viscoelastic characteristics. The extensional relaxation time λ is a measure of fluid elasticity in viscoelastic fluids such as dilute polymeric suspensions.

For mucosalivary fluids, major discrepancies and variability persist in the reported values of λ, with values ranging from 2.2 to 76.2 ms (Haward et al. 2011, Kesimer et al. 2010), while the density ρ and shear viscosity μ are close to that of water. In respiratory emissions (**Figure 5**), mucosalivary ligaments have diameters ranging, for example, from $d = 0.4$ to 1 cm, with associated capillary timescales $\tau = \sqrt{\rho d^3/\sigma}$, where σ is the liquid's surface tension. Here, τ ranges from 1 to 3.4 ms, leading to $0.65 \leq De \leq 78.7$, where $De = \lambda/\tau$ is the Deborah number quantifying the effect of viscoelasticity as the ratio of the polymer extensional relaxation to capillary timescales. Note that the mucosalivary ligaments are stretched by the background unsteady turbulent flow. The relative importance of viscous to inertial and surface tension forces is given by the Ohnesorge number, $Oh = \mu/\sqrt{\rho\sigma d} = \sqrt{We}/Re$, where $We = \rho u^2 d/\sigma$ is the liquid ligament Weber number,

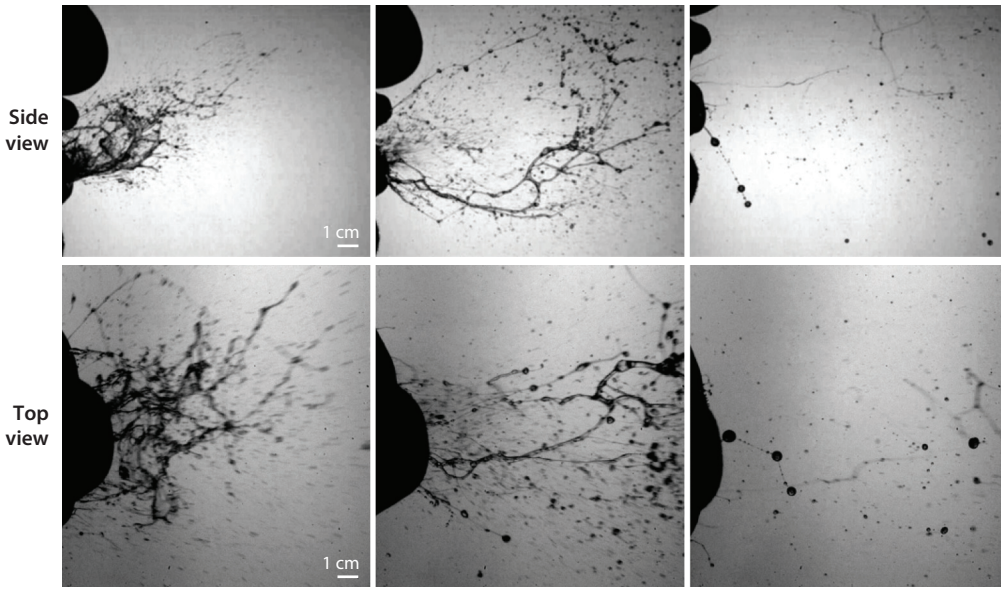

Figure 5

Fragmentation of mucosalivary fluid during a sneeze showing initial sheet formation and stretching (*left*); sheet piercing, resulting in sheet retraction in a rim, itself destabilizing into ligaments and beads on a string (*middle*); and ultimately the formation of droplets (*right*). The top view (*bottom row*) clearly highlights the sheets, their rupture into ligaments, and then finally the viscoelastic dynamics of extension and beads on a string, leading to the final selection of droplets via unsteady fragmentation. Photographs reprinted with permission from Scharfman et al. (2016), copyright 2016 Springer Nature.

for example, $\mathcal{O}(10^3)$ for a ligament of 0.2 mm moving at a speed of $u = 30$ m/s. For ligaments with diameters ranging from 0.2 to 0.6 mm, the Ohnesorge number is $Oh \approx 0.005$. Hence, the viscous effects are negligible compared to the inertial and surface tension effects for the emissions shown in **Figure 5**, although they may be important in subjects with respiratory pathologies. We expect viscous effects to be dominant, however, for pure mucus found deeper in the airways, and we expect this effect to vary over the course and with the type of an infection, thus reflecting a two-way coupling between the pathogen and the fluid phase (Zanin et al. 2016).

3.4. Exposure and Infection

In the context of respiratory diseases, the generation of mucosalivary droplets and their emission as part of the multiphase turbulent gas cloud, coupled with their evolution in the environment as governed by the multiphase droplet and phase-change physics of evaporation and condensation, form Phases 1–3 of our framework (**Figure 1**) and ultimately determine the nature, composition, and size of the droplets or droplet nuclei inhaled by a potential host (Phase 4). The size and composition of the inhaled particles determine not only the range and evolution (e.g., adhesion or resuspension) of the nuclei in the environment (Phase 3) but also the potential for penetration deep into the respiratory tract (Phase 4). Indeed, the size, composition, and pathogen load of inhaled droplet nuclei ultimately determine the target tissue that is reached in the lungs, from the large conducting upper airways to the smaller airways and ultimately the alveoli. Inoculation of animals, for example, has suggested that for the same viral load, the inhalation of an atomized solution results in higher infection and death rates than dry intranasal inoculation (Sonkin 1951, Wells

1955). The physics of deposition in the respiratory tract has been studied in the context of drug delivery and dosimetry of nebulizer treatments and has been discussed in reviews (e.g., Grotberg 2001). There remain important areas of open research to examine such deposition and penetration in the context of respiratory contaminated droplet residues as a function of their history from Phases 1–3 of the transmission process. In addition, rich questions remain open concerning the interplay between the transmission physics, the complex biochemistry, and the host immunology, including at the mucous barrier of the upper airway (Zanin et al. 2016), which is the first line of defense against respiratory infectious agents where the properties of pathogen-laden droplets shaped by their history in Phases 1–3 determine, in part, the success rate of host cell infiltration and infection.

3.5. Fluid Dynamics of Coronavirus Disease 2019

The COVID-19 outbreak has brought into sharp focus the central importance of the fluid dynamics of respiratory infectious disease transmission through exhalations, speaking, singing, coughing, or sneezing. Understanding this dynamics is particularly important for management of patient care settings where large numbers of symptomatic COVID-19 patients may release mucosalivary droplets into the environment. Additionally, medical procedures that create aerosols, such as intubations/extubations or oxygen delivery, can contribute to surface and air contamination. Finally, health-care providers may also be virus-shedding asymptomatic carriers contributing to transmission.

While reliable data on nosocomial SARS-CoV-2 transmission are lacking, some estimates suggest that 20% of confirmed COVID-19 infections in the United Kingdom occurred in patients hospitalized initially for conditions other than COVID-19 (Harding & Campbell 2020). A single-center case series of 138 COVID-19 patients in the Hubei province of China reported that person-to-person hospital-associated transmission of SARS-CoV-2 was suspected in 41% of the patients (Wang et al. 2020). Nosocomial transmission of the MERS coronavirus was also reported, likely from acutely ill long-term hospitalized patients (Majumder et al. 2017). While such estimates do not provide insights into the routes of transmission, it has been shown in laboratory experiments that SARS-CoV-2 retains infectivity for a minimum of 3 hours following aerosolization and for up to 72 hours on surfaces (van Doremalen et al. 2020). Additionally, an environmental sampling study of SARS-CoV-2 found the virus in the air vent of a symptomatic patient's hospital room, demonstrating the occurrence of long-range transport of viral particles (Ong et al. 2020), in conflict with the large-droplet theory of viral transmission, which assumes that large drops travel farthest, fall onto surfaces, and contaminate these surfaces only. In contrast, the discovery of viral particles in air vents is consistent with the multiphase turbulent gas cloud emission model, in which droplets are trapped within a gas cloud over long distances away from the patient before slowing down, enabling them to be advected by ambient air flows (at a few centimeters per second) for hours or days. The cloud emission model allows for pathogen-laden mucosalivary droplets to rapidly, on the order of seconds, reach distances of 5 to 8 m for unprotected coughs or sneezes, respectively.

However, despite the mounting evidence—or at least the possibility—of SARS-CoV-2 transmission through the air, the WHO, CDC, and other public health agencies have still resisted embracing measures to protect health-care providers and patients against this airborne transmission route, insisting that COVID-19 spreads primarily through large droplets settling on surfaces within 3 to 6 ft (1 to 2 m) from the source. While it is difficult or impossible to prove definitively, particularly during the ongoing pandemic, that airborne pathogen transmission plays an important role in COVID-19 transmission, the precautionary principle (SARS Comm. 2007, chapter 8)

would mandate providing hospital workers with the highest grade of personal protective equipment and, in particular, the N95 respirators that were in very short supply during the early stages of the pandemic in the Western hemisphere. In light of the recommendations by major public health agencies, one is left wondering whether the supply chain of personal protective equipment, rather than science and the precautionary principle, dictated infection control policy in the early stages of the pandemic.

In addition to elucidating the disease transmission process and informing policy makers about the merits of using masks (Bahl et al. 2020, Bourouiba 2020) and of novel materials for source control and reduction of resuspension of contaminants from protective equipment (Liu et al. 2020), fluid dynamic considerations can also inform other infection-control and return-to-work strategies. These include safety of medical procedures (e.g., aerosol-generating procedures or routine patient care in field hospitals during a pandemic); hand washing; social distancing requirements and, hence, limits on occupancy number and duration in various environments (Jones et al. 2020); decontamination innovations and indoor air hygiene strategies as made possible through ventilation types (Linden 1999, Hunt & Linden 2005); air filtration, decontamination, and conditioning systems; and localized flow control solutions. Indeed, flow heterogeneities are important in the transmission of pathogens indoors (Li et al. 2020). Hence, remediating airflow heterogeneities is important, as the well-mixed limit of indoor ventilation is inherently a maximum pathogen dilution limit, thus only providing the lowest possible bound of exposure risk given an indoor space. In fact, it is already known that such a limit needs to be revised in response to changes in indoor environments, including changes in buoyancy sources, such as occupants and equipment/devices, and fluctuations in venting (Vauquelin 2015) from naturally emerging oscillations, movement, door and window openings, etc., where buoyancy, geometry-dependent flows, and ventilation compete, potentially enabling the accumulation of contaminants in recirculation zones (Bolster & Linden 2007, Li et al. 2020). We will undoubtedly learn a lot over the coming months about how to optimize these nonpharmacological interventions and mitigation strategies to combat COVID-19 spread, as many governments around the world have begun loosening their lockdown orders and are hopefully planning to improve resilience against expected recurring waves of the pandemic by embracing the combined strategies of people–air–surface–space integrated management (Jones et al. 2020), including hand hygiene, surface cleaning, occupancy restrictions, indoor space and air management, and appropriate protective equipment, such as certain types of masks, for a given setting or activity.

4. NOSOCOMIAL PATHOGEN TRANSMISSION

Pathogens other than those transmitted by the respiratory route also transmit via the fluid and droplet phase. For example, about 23,000,000 infections and 50,000 hospitalizations are caused by noroviruses in the United States annually (Mead et al. 1999). As a leading cause of gastroenteritis-associated death, *Clostridium difficile* resulted in almost 500,000 infections and was responsible for approximately 29,000 deaths in the United States in 2011 (Lessa et al. 2015) and more than US$1.1 billion in cost per year (Kyne et al. 2002, Johnston et al. 2007). These numbers put *C. difficile* on par with deaths attributable to cancers of the ovaries, brain, or kidney (ACS 2019). The epidemic of Ebola virus disease in West Africa led to more than 2,000 deaths during the period from December 2013 to September 2014 (WHO 2014). All of these diseases share two of the most common symptoms for infection: diarrhea and vomiting. Recent evidence also suggests that these emissions could carry SARS-CoV-2, sampled in high loads from surfaces in patient lavatories (Ding et al. 2020, Liu et al. 2020).

Splashes from surfaces, sinks, or toilet flushes in hospitals or other indoor settings are often neglected routes of transmission, and to date there have been only rudimentary efforts at quantifying their effects. Shared bathrooms in hospitals, rehabilitation centers, or assisted living facilities are used by patients who might be infected, thus making them a likely source of indoor cross-contamination (Best et al. 2012, Liu et al. 2020). The pathogen-spreading potential of toilet flushes was investigated in toilets seeded with microorganisms that were later recovered from surfaces and in the air after flushing (Darlow & Bale 1959, Johnson et al. 2013b). The organisms in the bowl could not be fully cleared even after repeated flushing (Gerba et al. 1975), and the droplets produced by flushing harbored the organisms that were used for seeding, which remained airborne and viable. Recently, Johnson et al. (2013a) investigated different toilet designs and found that up to 145,000 sampled particles can be produced per flush. In North America, toilets in public places are often not fitted with lids, which are avoided particularly in patient-care settings to reduce surface contamination from biofilms or superbugs.

Despite the possibility of pathogen emission in bathroom settings, from flushes to water splashes from hand-washing, systematic studies of the source conditions and interfacial and multiphase fluid dynamics of such emission phenomena are currently lacking, as are designs for the reduction of secondary emissions and environmental contamination. Study of the relevant fluid dynamics of fragmentation and aerosolization can fill some of these gaps by directly characterizing the emission dynamics and spatiotemporal evolution of the spray and fragmentation processes involved. Recent direct visualizations (**Figure 6*a***) captured a toilet flush at 2,000 frames per second (C. Lu & L. Bourouiba, original data). Analysis of more recent data (C. Lu & L. Bourouiba, original data) revealed that a large number of droplet emissions are not visible to the naked eye ($d < 100$ μm) (**Figure 6*b***). These emissions account for more than 6 mL and can remain suspended in the air for a long time compared to the larger visible drops (with diameters up to 6 mm) that end up on surfaces. By visualizing, tracking, and quantifying the droplet trajectories, we can assess ranges of contamination, as illustrated in **Figure 6*b***. Some of these drops are emitted at high speed, $\mathcal{O}(10$ m/s), and are mostly emitted during the first 3 s of a typical 6-s flush, leading to local emitted Weber numbers as high as $We \sim \mathcal{O}(10^3$–$10^4)$ and possibly emitting additional secondary droplets upon impact via splashes.

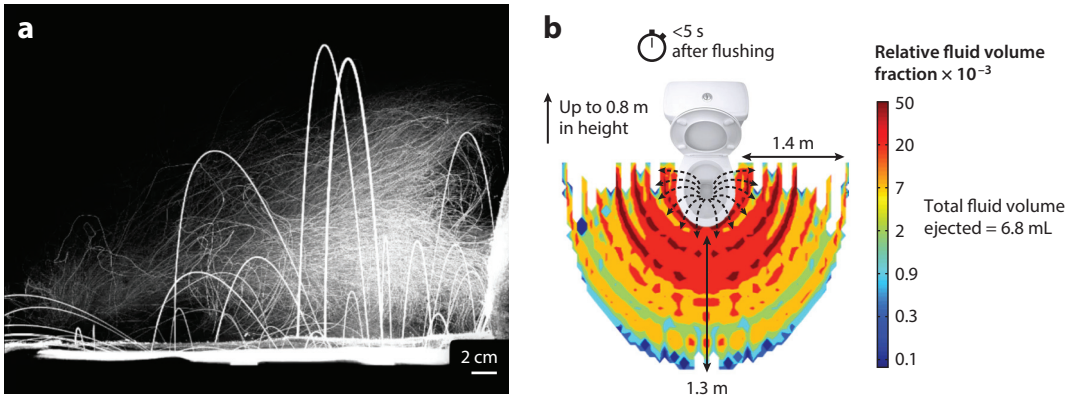

Figure 6

(*a*) High-speed imaging of droplet trajectories emitted from a high-pressure flush of a typical hospital toilet, showing ballistic trajectories for larger droplets and meandering droplet suspension for smaller ones (L. Bourouiba, original data). (*b*) Quantification and visual illustration of the projected relative surface and air contamination (up to 0.8 m above ground) from toilet flush emissions within 5 s after flushing (C. Lu & L. Bourouiba, original data).

The larger visible drops settle on surfaces within milliseconds, whereas the smaller, invisible drops are advected by local airflow (on the order of a few centimeters per second). Droplets settling on surfaces can be tackled in accordance with surface decontamination procedures of local infection control protocols. However, no system or protocol currently addresses air contamination. Furthermore, usual cleaning solutions not effective in neutralizing the most resistant pathogens, such as the spores of *C. difficile*, may even contribute to their dissemination by effectively lowering the surface tension, for example, down to 30 mN/m, compared to water at 72 mN/m, increasing the local Weber number and thus promoting fragmentation into either more or smaller droplets, depending on the fragmentation mechanism.

Nosocomial infectious disease transmission can be induced by a range of other ubiquitous fragmentation processes, from splashes in sinks to equipment decontamination and medical procedures. The fluid dynamic characterization of the sources of such emissions is complex and involves a combination of drop or jet impacts and sheet destabilization, in addition to bubble bursting, with a large number of secondary bubbles generated, for example, by the water decompression from pipes pressurized up to 80–90 PSI (552–620 kPa). We discuss the physics of bubbles and their role in generating secondary contaminated droplets in Section 5; other fragmentation processes are discussed in Sections 6 and 7.

5. WATER-TO-AIR TRANSFER AND BUBBLES AT THE INTERFACE

We have seen in prior sections how the underlying physics of interfacial and fragmentation dynamics elucidates a range of processes involved in pathogen dispersal and transmission. Organisms have also evolved to manipulate these processes for their own dispersal and proliferation (e.g., Zanin et al. 2016, Poulain & Bourouiba 2018, Ruhl et al. 2020). In this section we focus on such an interaction in the context of bubbles at the interface of a bulk fluid.

Air bubbles are ubiquitous at water surfaces (Walls et al. 2014). They are common in pools, toilets, and wastewater plants; are generated in industrial applications such as aeration and mixing; and are the outcome of natural processes such as wave breaking and rainfall on the oceans (Bourouiba & Bush 2013, Veron 2015). Bubbles can also cause public health concerns, as the droplets they generate from contaminated water may carry infectious payloads that can lead to airborne disease transmission (Blanchard 1989). Contaminated droplets can be easily transported over short and long distances by drafts and winds. In human and animal populations, inhalation of droplets or droplet nuclei containing bacteria is a recognized route of infectious disease transmission. For example, *C. difficile* nosocomial infections (Best et al. 2012) and outbreaks of *Legionella* (Prussin et al. 2017) and *Mycobacteria* (Falkinham 2003) have been linked to aerosolization from bursting bubbles.

A bubble at the surface of a fluid reservoir consists of a thin cap of water, $\mathcal{O}(10\ \mu\text{m})$ thick, entrapping air (**Figure 7**). The curvature of the cap induces an overpressure, $\Delta p \sim 2\sigma/R$, compared to the bulk water, where σ is the surface tension and R is the bubble cap radius. At first order, this pressure difference induces a drainage flow resisted by viscous stresses at the foot of the bubble, causing the cap to drain into the bulk to which it is connected and leading to a balance $\mu U/h^2 \sim \sigma/(R\,\ell)$, where h is the cap thickness, U is the drainage speed, μ is the viscosity, and ℓ is the length of the bubble cap foot (Lhuissier & Villermaux 2012). Hence, its thickness continuously decreases, and the cap eventually ruptures and ejects droplets (**Figure 7*d***). Upon initial rupture, a hole forms on the cap and grows at constant speed v, which can be related to the cap thickness h using the Taylor–Culick relation, $v = \sqrt{2\sigma/(\rho_w h)}$ (Taylor 1959, Culick 1960), with ρ_w the water density.

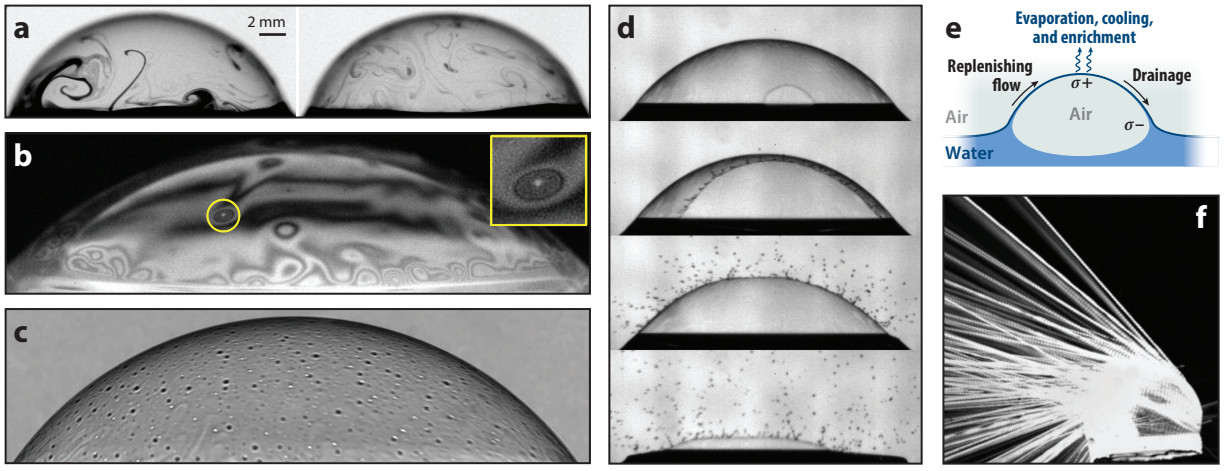

Figure 7

(*a*) Once gently deposited as a drop on the surface of a young bubble, potassium permanganate mixes and forms lamellae that elongate and overlap in an ever-weakening stirring field. (*b*) A bubble of salt water at ambient humidity lives as long as minutes, and as the salt concentrates, crystals form and slide down the bubble cap (*highlighted inset*). (*c*) Schlieren imaging of a bacteria-laden bubble showing the persistence of organisms on the cap over the contaminated bubble's full lifetime, which is lengthened by bacterial secretions. Optical methods such as Schlieren imaging, shadowgraphy, and interferometry reveal the subtle dynamics on the bubble cap and help track the location and number of bacteria on the cap (Poulain & Bourouiba 2018, Su 2018). (*d*) The increase in the bubble's lifetime (here about 55 s) leads to an increase in the number of droplets emitted due to more violent destabilization of the receding rim formed from the rupture of older and thinner bubbles. Bubble cap radius in panels *b–d* is ∼5.6 mm. (*e*) The mechanisms extending the lifetime of a bubble inherently involve a Marangoni flow from the foot to the apex that counters the curvature-induced drainage of the bubble film. This counterflow can be induced by several conditions that locally increase surface tension (σ) at the apex, including temperature gradients (e.g., bubbles emerging into colder atmospheres), evaporative cooling (e.g., bubbles emerging in nonsaturated local environments), and chemical or biological compound gradients (e.g., evaporation at the apex leading to the local enrichment of certain compounds such as salt). The secretions of organisms, even those not known for biofilm secretion, also increase the lifetime of bubbles (Poulain & Bourouiba 2018). Panel *e* reproduced from Poulain & Bourouiba (2019), with the permission of the American Institute of Physics. (*f*) Droplets generated from older bubbles tend to be smaller, are emitted at higher speeds, are more easily advected by ambient air flows or winds away from the boundary layer, and hence may escape the interface region more easily than droplets generated by younger bubbles. Photographs adapted with permission from (*a*,*b*) Poulain et al. (2018), copyright 2018 Cambridge University Press; and (*d*) Poulain & Bourouiba (2018), copyright 2018 American Physical Society.

Important factors governing the properties of the ejected droplets are the thickness of the cap at burst and the mixing that occurs on the surface of such bubbles during the bubble's aging process (**Figure 7*a***). Thinner (typically older) bubbles emit more, smaller, and faster droplets than thicker (typically younger) bubbles. This is due to the higher acceleration reached upon cap opening for thinner films, leading to a more violent rim destabilization (Rayleigh–Taylor instability). This is also true for bubbles contaminated with microorganisms that, as we show in **Figure 7*c***, stay on a bubble cap throughout the bubble's life. Such older bubbles can launch hundreds of contaminated droplets upon burst (**Figure 7*d***) (Poulain & Bourouiba 2018).

Capillary length: length scale relating surface tension to gravitational force; $\ell_c = \sqrt{\frac{\sigma}{\rho_w g}}$

At the surface of distilled, bottled, or clean tap water, bubbles burst very quickly. While their lifetimes vary, most burst within a couple of seconds, and typically less than 5% survive up to 10 s. From balance of curvature-induced pressure-driven outflow and viscous stresses at the foot, coupled with mass conservation, we obtain a drainage-dominated thinning law of the film thickness, namely, $-\mathrm{d}h/\mathrm{d}t \sim \sigma/\mu \cdot \ell_c/R \cdot (h/R)^{5/2}$, where $\ell_c = \sqrt{\sigma/\rho_w g}$ is the capillary length and g is the gravitational acceleration. The thinning law results in the decay of bubble film thickness as $h(t) \sim t^{-2/3}$ with time t. However, even during their short lifetimes at the interface, the interaction

of bubbles with the ambient air can affect their thickness in a surprising and counterintuitive manner. By cooling the bubble cap apex, evaporation increases surface tension at the apex compared to that of the bubble foot, which remains at ambient temperature (**Figure 7*e***). This imbalance in surface tension drives water from the foot (low surface tension) toward the cap (high surface tension) via a thermal Marangoni flow. This upward flow acts against the drainage of the bubble film. Hence, for clean bubbles of a given age, evaporation leads to thicker bubbles. This replenishing effect of evaporation is in fact general. Any mechanism leading to a relatively higher surface tension at the bubble apex relative to the foot increases the age and thickness of clean bubbles. This effect can be caused by differences in temperature between bulk fluid and bubble cap apex by cap evaporative cooling, and by chemical or biological compound gradients. It can also be exacerbated by volatile compounds such as alcohol (Lohse & Zhang 2020) and salts, with important implications for the ocean–atmosphere coupling. All of these cases lead to thicker bubbles that continue, however, to thin as $t^{-2/3}$ (Poulain & Bourouiba 2018, 2019; Poulain et al. 2018). Interestingly, bacteria also release secretions that stabilize bubbles, making them resistant to surface perturbations that would otherwise cause clean bubbles to burst at much shorter lifetimes. The effect of such secretions is similar to that of surfactants, the molecules that allow soap bubbles to last for a very long time (Poulain & Bourouiba 2018).

Thicker caps are, on average, more resilient to intrusions or Marangoni-induced localized divergent perturbations (Néel & Villermaux 2018, Poulain et al. 2018), leading to bubbles that live longer on average. Stabilization of the interface via surface-active compounds can provide increased elasticity of the interface and longer bubble lifetimes. If such bubbles do live long enough, on the order of 30 s or minutes, their thickness becomes sufficiently small for the capillary drainage thinning, $-\mathrm{d}h/\mathrm{d}t \sim h^{5/2}$, to become dominated by evaporative thinning, $-\mathrm{d}h/\mathrm{d}t \sim (J/\rho_\mathrm{w})$, where J [kg/(m^{2}s)] is the constant flux of water vapor per unit bubble area (**Figure 8**). The transition between the drainage-dominated and the evaporation-dominated regimes occurs at a critical bubble cap thickness h_c and time t_c, such that

$$h_\mathrm{c} \sim R\left(\frac{R}{\ell_\mathrm{c}}\frac{J/\rho_\mathrm{w}}{\sigma/\mu}\right)^{2/5} = \mathcal{O}(1\ \mu\mathrm{m}),$$

$$t_\mathrm{c} = t(h = h_\mathrm{c}) \sim \frac{\mu h_\mathrm{c}}{\sigma}\left(\frac{\sigma/\mu}{J/\rho_\mathrm{w}}\right)^{1/5} = \mathcal{O}(10\text{–}20\ \mathrm{s}),$$

where the evaporation flux, $J \sim (1 - H)$, is a function of ambient relative humidity H; thus, we have $h_\mathrm{c} \sim R^{2/5}(1 - H)^{2/5}$ (Poulain & Bourouiba 2018, 2019). This regime shift is important for understanding how contaminated bubbles that have lifetimes longer than 10–20 s produce contaminated droplets most efficiently. This subtle competition between the direct removal of water by evaporation and the replenishing effect of Marangoni flows induces a longevity-triggering shift in the thinning law, which turns out to have important implications for water-to-air pathogen transfer (Phase 2 in **Figure 1**). Older, biologically contaminated bubbles (on the order of 60 s), for example, can produce 10 times as many droplets as a young bubble. These droplets are one-tenth the size of (as small as 10 μm in radius) and emitted up to 10 times faster than (up to 15 m/s) the droplets produced by clean young bubbles (Poulain & Bourouiba 2018, 2019; Poulain et al. 2018), supporting the view that pathogens could have evolved to manipulate the fluid phase to enhance their own dispersal.

Some bacteria are known to produce biofilms that can be protective to them. However, the effects of bacterial secretions on bubbles arise even for bacteria such as *Escherichia coli* that are not known to produce biofilms. The effect of their secretions on bubbles is measurable in the

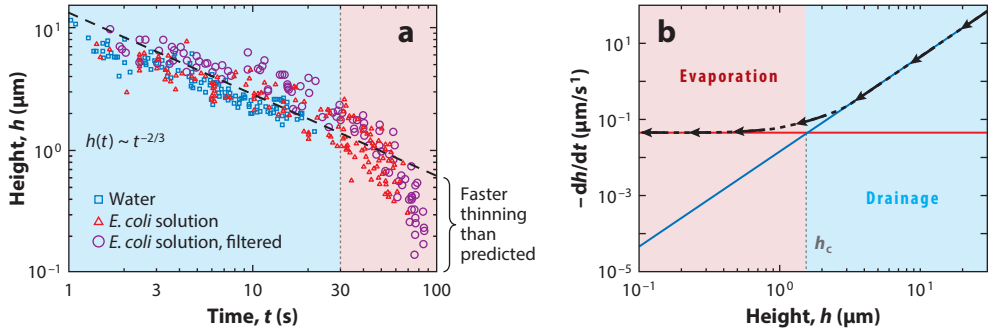

Figure 8

The competition between two bubble-thinning mechanisms important at different timescales. The earlier part of a bubble's life (*blue regions*) is dominated by thinning governed by drainage from the balance of capillary pressure-driven flow and viscous stresses at the foot of the bubble, leading bubble thickness to decrease as $h \sim t^{-2/3}$ (*a*), with the magnitude of the thickness also influenced by Marangoni effects (Poulain et al. 2018). However, surfactants or secretions from organisms significantly enhance bubble lifetimes, resulting in a transition in the thinning law to one dominated by evaporation (*red regions*). Such a transition occurs at timescales on the order of $t_c \sim \mathcal{O}(10\text{ s})$ and at associated thicknesses on the order of $h_c \sim \mathcal{O}(1\ \mu\text{m})$ (*a*,*b*). The reason such a transition occurs is that the short-time drainage governed by the balance of capillary pressure–driven flow and viscous stresses decreases in magnitude as the film thickness decreases (*gray arrows* in panel *b*), yet the evaporative flux out of the film is constant throughout. Eventually, as the film thickness becomes small enough, the evaporative flux–induced thinning becomes dominant (*b*). Surfactants and bacterial secretions enhance bubble longevity even when they induce no measurable change in static surface tension, highlighting the important effect of minute changes in film property fluctuations. As a result of this regime transition, contaminated bubbles live longer and reach critical thicknesses that enable, upon rupture, the ejection of smaller and faster droplets than noncontaminated bubbles, enhancing dispersal of microorganisms at the water–air interface. Figure adapted with permission from Poulain & Bourouiba (2018), copyright 2018 American Physical Society.

bubble lifetime and thinning laws (e.g., **Figure 8**), even when the contaminated fluid's static surface tension does not change, as measured within ±2% accuracy via the pendant-drop method. Hence, despite their tiny size, seemingly low concentrations, and negligible effect on the fluid's static surface tension, pathogens cannot be assumed to be passively transported in fluids without affecting the fluid physical processes of the medium carrying them. Instead, Poulain & Bourouiba (2018) have shown that when microorganisms contaminate bubbles, they can subtly manipulate the underlying interfacial physics to optimize their long-distance dispersal.

6. AGRICULTURE AND FOOD SAFETY: FLUID FRAGMENTATION IN FOLIAR DISEASE TRANSMISSION

Diseases of crops can have a significant effect on yield, with potentially historical consequences, such as the mass migration and estimated one million deaths during the 1845 famine caused by infestation of the potato plant by *Phytophthora infestans* (Mokyr 2020). Around 10% of the world crops are still lost annually to plant diseases, with an estimated cost of billions of dollars, which typically puts disproportionate pressures on resource-limited communities (Fones & Gurr 2015). Plant and crop diseases also affect human health, as plant diseases are responsible for up to 60% of annual wheat loss (Park 2007), aggravating the conditions of the one billion malnourished individuals worldwide (Strange & Scott 2005).

Epidemics in the plant and agricultural worlds depend on the dispersal and transport of pathogens between plants and fields, for which Phases 1–4 of **Figure 1** apply. The dispersal can involve long-distance mechanisms across large regions via established atmospheric patterns or rare events such as hurricanes. Dispersal can also involve reconfiguration of soil or landscapes

induced by erosion and surface runoff. Since the physics of long-distance dispersal or erosion has been covered elsewhere (Römkens et al. 2002, Furbish et al. 2007, Wei et al. 2014, Wang et al. 2018b, Roper & Seminara 2019), our focus here is on the host-to-host (intermediate) scale of rainfall-induced pathogen transmission.

When trapped in sticky mucilage, spores and bacteria can only be dispersed via interaction with a liquid phase (Meredith 1973, Aylor 2017), and rainfall has been identified as a common precursor of foliar disease outbreaks: Lesions on crops have been observed a few weeks after rain events (Reynolds et al. 1987, Geagea et al. 1999, Paul et al. 2004, Aylor 2017), and new lesions at the bottom of wheat leaves appeared following rainfalls and preceded outbreaks of *Septoria tritici*, *Septoria nodorum*, yellow rust, and tan spot (Fitt et al. 1989, Huber & Gillespie 1992). In a laboratory setting, simulated rain resulted in the contamination of the surroundings of an infected plant (Geagea et al. 1999). To build on these observation and develop generalizable approaches for different canopies and rain intensities, researchers need physical models of the rain/irrigation–leaf interaction. This is also valuable for optimizing produce decontamination postharvest. Such modeling requires elucidation of the physical mechanisms that govern pathogen dispersal, which is vital for the monitoring, prediction, and control of foliar disease epidemics. Additionally, optimization of timing and amount of sprayed chemicals requires improved understanding and modeling of the multiscale spray physics and of the spray–crop interaction to minimize losses in the form of spray drift (Hewitt 2000). However, studies of pathogen dispersal by rain splash have been mostly statistical in nature, with simulation models generally based on empirical approaches in which the physical mechanisms are not resolved (Madden et al. 2007).

6.1. Leaf Wetting and Fluid Fragmentation Modes

Pathogen dispersal through raindrop impact on real contaminated leaves is a complex event that couples the fluid dynamics of the rain drop to the biophysical properties of the pathogen and the biomechanical properties of the leaf (**Figure 9**). Indeed, the rapid local dynamics of drop impacts on leaves is affected by various morphological (size and margin shape) and mechanical (weight and compliance) characteristics that shape the patterns of contamination around plants (**Figure 10**). Additionally, surface properties, such as roughness, venation pattern, and the leaf's wetting properties, are important factors determining the local transmission dynamics. In particular, the leaf's wetting characteristics determine whether—after rain, irrigation, or dew dripping—leaves are likely to be laden with sessile drops or coated by films. Indeed, the prior physical picture of rain-induced contamination dispersal mostly considered the two extremes of very low-wetting (superhydrophobic) surfaces (Josserand & Thoroddsen 2016) or very high-wetting surfaces, resulting in a film coating the leaves (Fitt et al. 1989). However, considering about 30 common plants, Gilet & Bourouiba (2014) found contact angles to vary between 60° and 120°, suggesting that it is critical to consider how leaves of intermediate wetting affect raindrop–leaf interactions and hence the footprint of contamination (**Figure 9**).

Given such common intermediate wetting for crop leaves, coupled to a leaf's morphological and biophysical characteristics, Gilet & Bourouiba (2015) identified two dominant modes of unsteady fluid fragmentation distinct from the prior physical picture of impact on fully wetted leaf surfaces (**Figure 9**): (*a*) crescent-moon fragmentation (**Figure 11*a***), with direct, splash-like drop-on-drop interactions involving mixing between the impacting drop and the sessile drop; and (*b*) inertial detachment fragmentation (**Figure 11*c***), with indirect, drop–leaf–drop interactions between the impacting drop and the sessile-contaminated drop; fluid fragmentation driven by the momentum imparted to the leaf upon raindrop impact; and little to no mixing between the drops, possibly creating undiluted emissions from the infected host. Thus, wetting combined with mechanical foliar

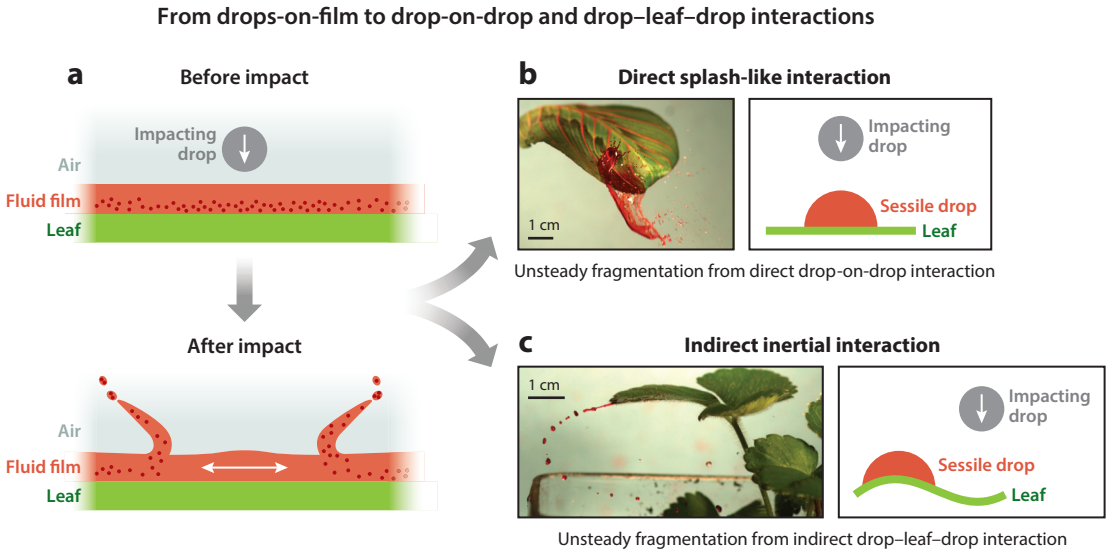

Figure 9

The shift in the physical picture for rain-induced disease transmission in plants, from the view of leaves coated by films (Fitt et al. 1989) to the dominant role of average wetting with sessile drop–laden leaves (Gilet & Bourouiba 2014). Instead of dispersal from splashes on thin films (*a*) (Yarin 2006, Eggers & Villermaux 2008), the intermediate wetting of leaves and their range of compliance and inertia enable two dominant modes of unsteady fluid fragmentation (Gilet & Bourouiba 2015): (*b*) crescent-moon fragmentation, with direct interaction and mixing between a sessile drop and an impacting one (Wang & Bourouiba 2017), and (*c*) inertial detachment with stretched ligament breakup, involving an indirect interaction between the impacting and contaminated sessile drops, with fluid fragmentation driven by the momentum imparted to the surface or leaf upon raindrop impact. Panel *a* adapted with permission from Fitt et al. (1989), copyright 1989 Annual Reviews; photographs in panels *b*,*c* reprinted with permission from Gilet & Bourouiba (2015), copyright 2015 the authors.

properties defined a new framework for leaf-to-leaf transmission, moving from a physical picture of crown-type vertical sheet fragmentation dynamics to two dominant modes of contaminated fluid emissions. How can we know a priori which of the two mechanisms (**Figure 9**) dominates?

6.2. Leaf Mechanics and Fragmentation Select Mode of Pathogen Emission

Gilet & Bourouiba (2015) introduced a new dimensionless compliance parameter, $\alpha = v_L/v_f$, where v_L is the leaf velocity at the impact point and $v_f = 2R/t_f$ is the velocity of fluid fragmentation. Here, R is the radius of the sessile drop on the leaf, and t_f is the fragmentation timescale, which is expected to vary with the sessile drop size and is on the order of the corresponding capillary timescale, $t_f \sim \sqrt{M/\sigma}$. Here, σ is the surface tension of the fragmenting fluid, and M is the mass of the sessile drop in the case of inertial detachment without mixing of the impacting and sessile fluids, or a combination of the masses of the sessile and impacting drops if full mixing occurs. The value of α can be measured for plants and canopies of interest or estimated on the basis of mechanical characteristics of the leaves (Gilet & Bourouiba 2015). An average value, $\bar{\alpha}$, can also be estimated for the canopy to include the combined compliance of the leaves and stems when the effects of the latter are nonnegligible.

The value of α captures the influence of leaf size and compliance on the dominant mode of fragmentation—direct or indirect in **Figure 9**—for leaves of intermediate wetting. Thus, α determines the footprint of contamination around the plant (**Figure 10**): Increasing α reduces the range of the pathogen footprint. Indeed, more compliant leaves would be expected to divert part

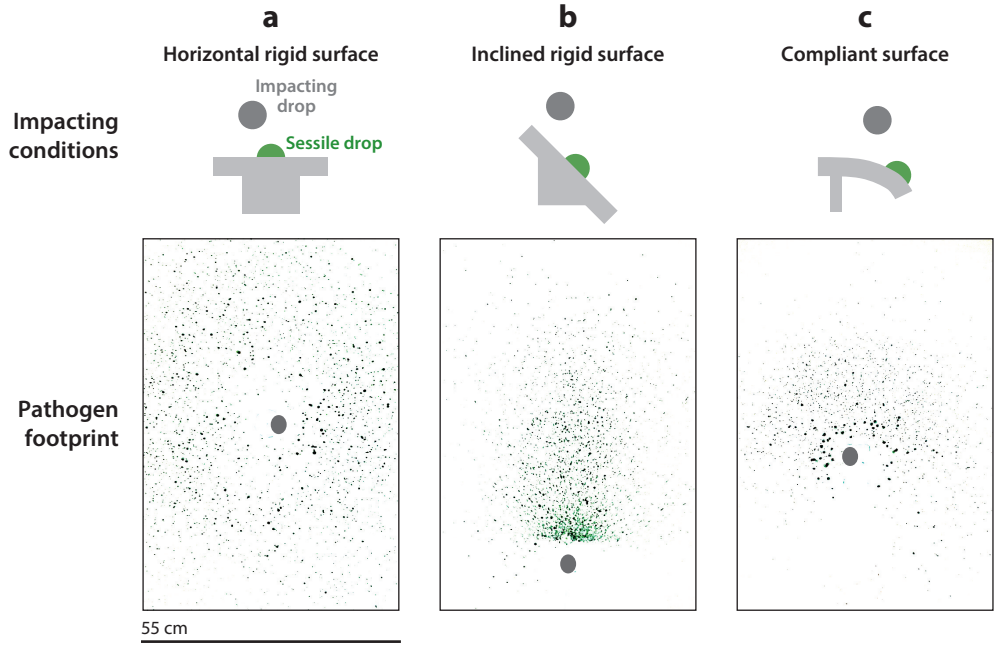

Figure 10

Local, small, and rapid fragmentation processes shape the larger-scale pathogen footprint of contamination (Gilet & Bourouiba 2015). (*a*) Impact of a drop on a rigid surface with a sessile drop at the edge leads to crescent-moon fragmentation and an isotropic contamination footprint around the target. (*b*) An inclined rigid surface provides additional forward velocity to the ejected droplets, resulting in a directional footprint of contamination around the target. (*c*) Compliance changes the footprint of contamination around the target, not only providing a forward component added to the speed of ejection due to the bending of the substrate but also affecting the droplet sizes produced, which result from a combination of crescent-moon (**Figures 9*b*** and **11*a***) and inertial detachment fragmentation (**Figures 9*c*** and **11*c***).

of the impacting kinetic energy, at a given Weber number of impact, toward elastic deformation of the plant, as suggested in **Figure 10*c***. However, a closer look reveals a more subtle effect, namely, that above a certain threshold value, $\alpha^* \approx 4$, the system enters a new regime in which the inertial detachment fragmentation mode (**Figure 11*c***) becomes possible. When inertial detachment emerges, this new mechanism of fragmentation and ejection can enhance the range of deposition of larger contaminated droplets. Indeed, when both direct (crescent-moon) and indirect (inertial detachment) modes of fragmentation coexist, the latter produces larger droplets and projects farther than crescent-moon splashes can in the same regime of α. This insight is important, as large ejected droplets are suspected to lead to a higher probability of infection of a healthy leaf due to the localized deposition of a higher concentration of the pathogen. (Note that the same argument is not necessarily true for human diseases, particularly when inhalation is concerned, as smaller droplets or droplet nuclei may enter deeper into the respiratory system where defense mechanisms, such as the mucous barrier and clearance, might be weaker.) In other words, increasing leaf compliance appears at first to monotonically decrease the range of pathogen-bearing droplets ejected from a sick plant. This decrease in apparent efficiency of transmission in terms of range is mitigated by the emergence of the inertial detachment fragmentation mode for high enough compliance, which increases the risk of successful infection due to the larger drop sizes and their higher potential pathogen load (due to reduced dilution upon fragmentation for inertial detachment fragmentation). Ultimately, the range of contaminated drops, and thus risk of silent

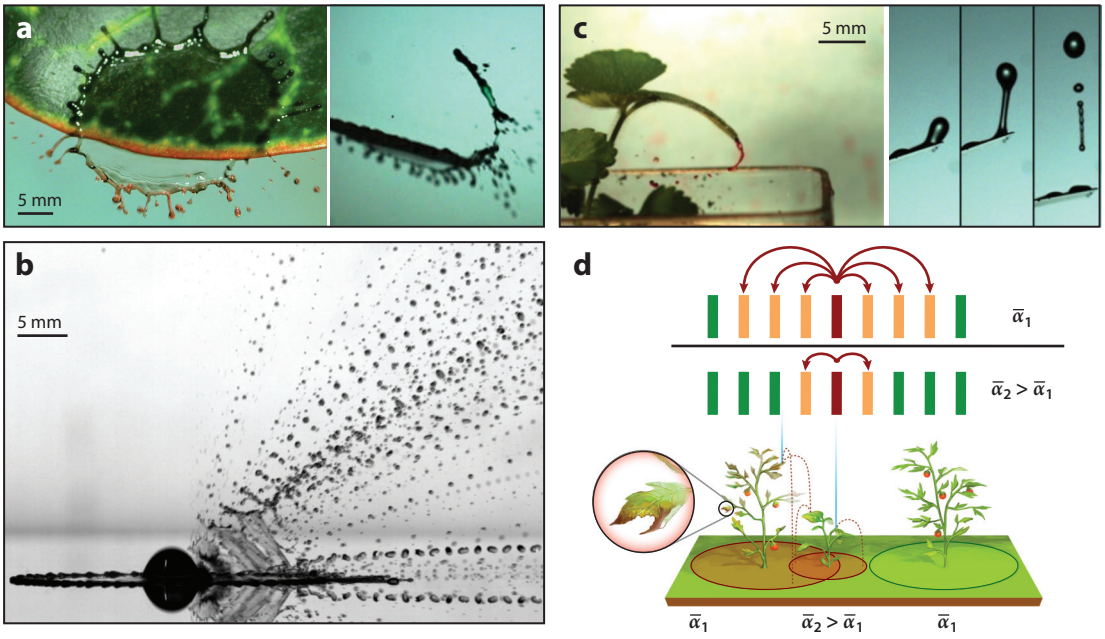

Figure 11

Removal of pathogens from leaves where pathogen ejection is governed by fluid–structure interactions during rainfalls. (*a*) Crescent-moon fragmentation leading to the formation of a sheet rising upward upon impact onto a sessile drop and producing stretching and fragmentation into droplets of high outward velocities ejected away from the impact point, with secondary droplet formation and ejection at speeds higher than the original drop impact speed. Photographs reprinted with permission from (*left*) Wang & Bourouiba (2018a), copyright 2017 Cambridge University Press; and (*right*) Gilet & Bourouiba (2015), copyright 2015 the authors. (*b*) Secondary droplet speeds reaching 9 m/s, or about 1.5 times the speed of the original impacting drop, for an impact with a Weber number of $We = 2{,}400$. (*c*) Alternative fragmentation from impact on leaves can include the inertial detachment, which is only possible for leaves with sufficient compliance parameter, $\bar{\alpha}$. (*d*) Fluid dynamics of pathogen-bearing droplets and contamination provide insights into the expected speed of an epidemic front in a field of known crops, regardless of the specificity of the organism, at first order. Moreover, the fluid–structure interaction and fluid fragmentation and mixing allow one to leverage the inherent mechanical properties of crops to effectively alternate them in organic fields or polyculture fields in cases where chemical or bioengineering mitigation methods are limited or cannot be used (Gilet & Bourouiba 2015). Panel *d* adapted with permission from Gilet & Bourouiba (2015), copyright 2015 the authors.

contamination or epidemic spread in a field, can be computed from the dominant modes of emission from fluid fragmentation ($\bar{\alpha}$ value) and by accounting for drag and evaporation. The range and pattern of contamination can be further refined by accounting for the boundary layer flow inherently induced by the local density, morphology, and configuration of the plants and canopy (Aylor 2017).

These insights open new pathways for field planning. For a fixed plant density, a higher $\bar{\alpha}$ value would lead to a higher epidemic reproduction number, R_0, in the field (Madden et al. 2007), as each contaminated plant would lead to more secondary infections per rainfall or irrigation event (**Figure 11*d***). Moreover, the insights gained allow for a reconsideration of polyculture by alternating crops based not just on their immunological diversity against a given known pathogen, but also on their intrinsic mechanical and surface properties to create a firewall around high-value crops (high versus low $\bar{\alpha}$ values) by sufficiently spacing out high-value crops to mitigate transmission while utilizing the gaps for other crop cultures (**Figure 11*d***). The advantage of this approach is that the firewall would not necessarily be protective against a specific suspected pathogen but

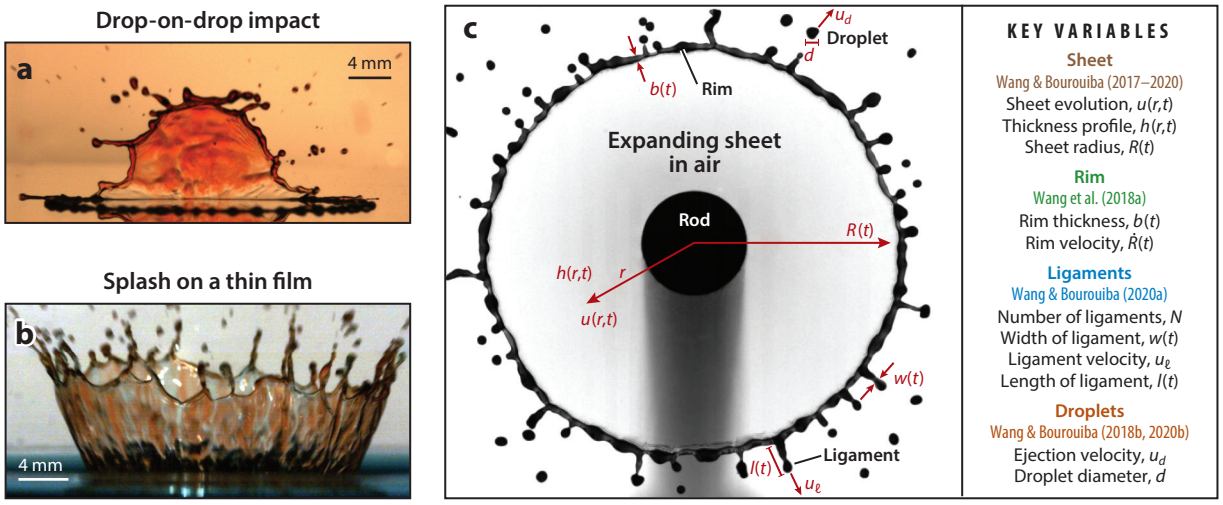

Figure 12

Universality in unsteady fluid fragmentation. (*a*) Crescent-moon fragmentation from a drop-on-drop impact (Gilet & Bourouiba 2015). (*b*) Splash on a thin film. (*c*) Sheet expansion from impact on a surface of comparable size to that of the impacting drop (Wang & Bourouiba 2017), illustrating the canonical system of an expanding sheet in the air, with thickness $h(r, t)$, inner radial velocity $u(r, t)$, and radius $R(r, t)$, bounded by a rim of thickness $b(t)$. Ligaments of width $w(t)$ and length $l(t)$ grow along the rim with mass outflux q_{out} and eject droplets of diameter d and speed u_d. The prediction of droplet sizes and speeds emitted throughout the unsteady fragmentation process requires understanding the coupled physics of the sheet, rim, and ligament formation and shedding. Panel *c* adapted with permission from Wang & Bourouiba (2020a), copyright 2020 Cambridge University Press.

could reduce propagation of a larger class of rain- or irrigation-induced diseases in a given field while also allowing for efficient intercrop spacing.

The insights gained also have implications for broader mechanisms of fluid and pathogen deposition/retention (e.g., irrigation contamination of produce by human or plant pathogens), ejection (e.g., pathogen dispersal upon irrigation or rain), or removal from leaves of complex shapes (e.g., postharvest decontamination for food safety). In all such applications, the complex leaf geometry results in a nonaxisymmetric liquid sheet fragmentation in the air, with distinct drop size and speed distributions compared to axisymmetric sheet fragmentation (Lejeune et al. 2018) (**Figures 10**, **11*a*,*b***, **12*a***, **13*b***). Although different in configuration, crown splashes upon drop impact on a thin film (Roisman & Tropea 2002, Josserand & Zaleski 2003, Berberović et al. 2009) or a deep pool (Zhang et al. 2012, Agbaglah et al. 2015), crescent-moon splashes (Roisman et al. 2002, Gilet & Bourouiba 2015, Wang & Bourouiba 2018a) (**Figures 11*a*,*b*** and **12*a***), or impacts close to edges of surfaces (Lejeune et al. 2018) (**Figures 11*a*** and **13*b***) all involve unsteady sheet formation and fragmentation. Above a certain threshold Weber number, the impact transforms the drop bulk volume into an expanding sheet of time-varying velocity and thickness, bounded by a moving rim of time-varying thickness that destabilizes into droplets (Eggers & Villermaux 2008) (**Figure 12*c***). Similarly, respiratory fluid fragmentation, discussed in Section 3.3 (**Figure 5**), also involves a similar sequence, from sheets, to rims, to drops. Given the universality in the steps of fragmentation, it becomes clear that quantifying and predicting, with high accuracy, a canonical unsteady fragmentation process of reduced complexity is required to tackle the key challenges of emission and transport of pathogens in a range of populations and disease systems. One such process emerges from drop impact on a target of comparable size to that of the impacting drop, namely, the dynamics of canonical unsteady sheet fragmentation, which we discuss next (**Figure 12*c***) (Wang & Bourouiba 2018a,b, 2020a,b; Wang et al. 2018a; Y. Wang & L. Bourouiba, manuscripts in review).

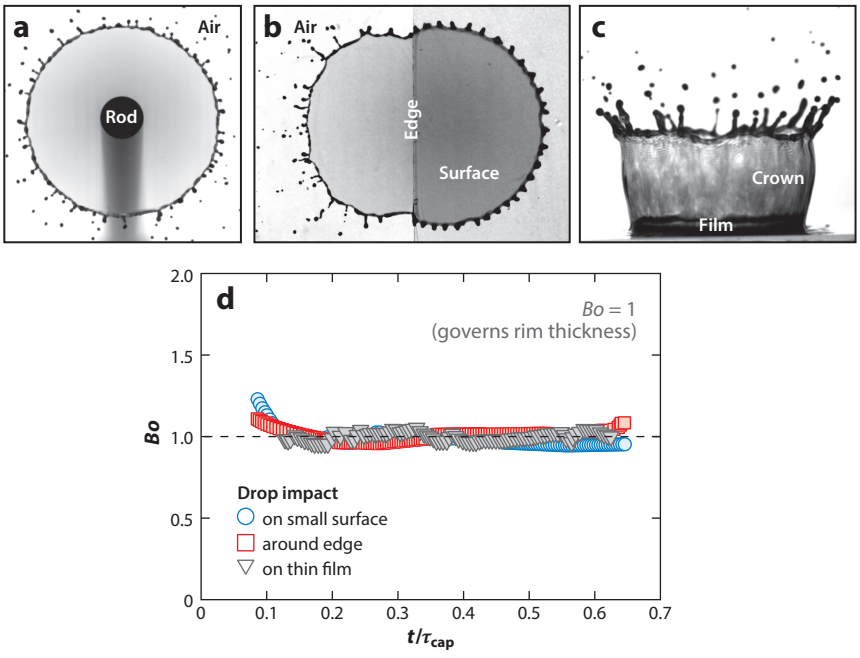

Figure 13

Three unsteady fluid fragmentation processes: (*a*) drop-on-pole, (*b*) drop-on-edge, and (*c*) drop-on-film fragmentation for which (*d*) the rim thickness is governed by the local Bond number criterion, $Bo(t) = 1$, despite the difference in experimental conditions (Wang et al. 2018a). Figure adapted with permission from Wang et al. (2018a), copyright 2018 American Physical Society.

7. UNSTEADY FRAGMENTATION: DROPLET SIZES AND SPEEDS SHAPING TRANSMISSION

Throughout this review we observed that fluid properties and their fragmentation behavior shape the phases of transmission and contact (**Figure 1**) for a variety of pathogens and host systems (**Figure 2**). They select for droplet sizes, speeds, and pathogen or contaminant payload, all governing the transport, persistence, and infectivity of the pathogens during the obligatory phase of host-to-host transmission to which organisms surely adapted in order to maintain the cycle of infection on which their survival depends. We note that short-lived unsteady fluid fragmentation processes bestow upon droplets, via a series of coupled interfacial instabilities, time-varying characteristics that are important determinants for assessing the risk of contamination and hence for controlling the chain of transmission. This is in contrast to steady fragmentation (Clanet & Villermaux 2002, Bremond & Villermaux 2006, Villermaux 2007, Déchelette et al. 2011), for which the properties of the spray droplets are independent of time or all formed simultaneously.

The canonical two-dimensional (2D), axisymmetric unsteady fragmentation process resulting from drop impact on a target of comparable size results in rich, coupled, and spatially and temporally varying multiscale nonlinear processes, which in the following sections we break down into the problems of sheet and rim evolution and the distributions of droplet size and speed.

7.1. Canonical Unsteady Fragmentation System: Sheet Dynamics

The combination of experimental approaches and high-accuracy feature extraction and tracking, coupled with interfacial flow theory, has helped elucidate the instabilities governing the selection

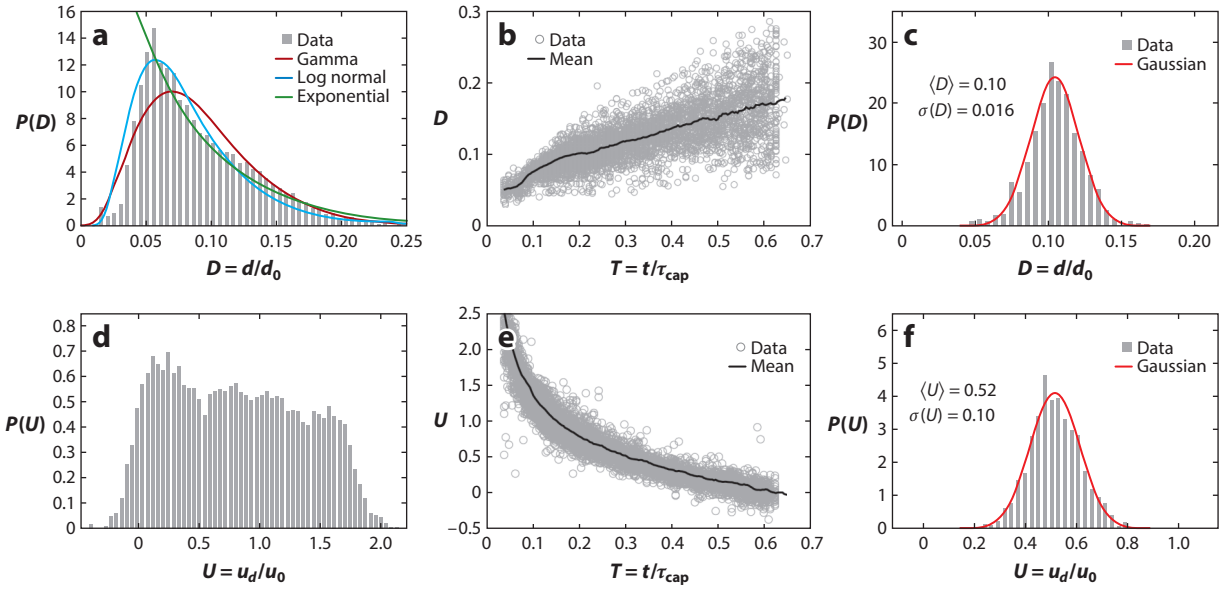

Figure 14

The important role of unsteadiness in shaping the droplet sizes and speeds from unsteady fluid sheet fragmentation. (*a*,*d*) Skewed overall probability density functions of droplet size, $D = d/d_0$ (*a*), and speed, $U = u_d/u_0$ (*d*), normalized by the impacting drop size, d_0, and impact speed, u_0, for Weber number $We = \rho u_0^2 d_0/\sigma = 963$. Here, ejected droplet sizes and speeds were measured throughout the fragmentation process. (*b*,*e*) Clear time variation, or unsteadiness, of the instantaneous ejected droplet sizes D (*b*) and speeds U (*e*) over time. Here, time is normalized by the capillary time, $\tau_{cap} = \sqrt{\rho d_0^3/\sigma}$. Unsteadiness clearly shapes the skewness of the final cumulative distributions (*a*,*d*). Indeed, the instantaneous size (*c*) and speed (*f*) distributions are in fact narrow and well captured by symmetric Gaussian distributions throughout the fragmentation, as shown here for droplets in flight at $T = t/\tau_{cap} = 0.4$. It is a superposition of narrow and symmetric Gaussians with moving means that governs the skewness and shape of the overall distribution of sizes (*a*) and speeds (*d*) from unsteady fragmentation (Wang & Bourouiba 2018a,b; Wang & Bourouiba 2020a,b; Y. Wang & L. Bourouiba, manuscripts in review). Figure adapted with permission from Wang & Bourouiba (2018b), copyright 2018 Cambridge University Press.

of droplet size and speed distributions in unsteady fragmentation (**Figure 14**). Starting with the sheet dynamics, light absorption (Vernay et al. 2015, Wang & Bourouiba 2017) and particle tracking have confirmed that the unsteady sheet velocity flow profile, $u(r, t)$, behaves as $u(r, t) = r/t$. Similarly, Wang & Bourouiba (2017) derived and validated a universal unified thickness profile, $h(r, t) \sim t/(a_3 r^3 + a_2 r^2 t + a_1 r t^2)$, for the sheet in air (**Figure 12*c***), where the a_i are fixed and independent of impact Weber number. The profile reconciles two competing profiles proposed in the literature: $h(r, t) \sim t/r^3$ (Rozhkov et al. 2004) and $h(r, t) \sim 1/(rt)$ (Villermaux & Bossa 2011). The full closed-form prediction of the unsteady droplet size and speed distributions requires such a unified thickness profile, as well as additional insights (**Figure 12*c***) on rim dynamics and coupled ligament–drop systems (Wang & Bourouiba 2020a,b; Y. Wang & L. Bourouiba, manuscripts in review).

7.2. Canonical Unsteady Fragmentation System: Rim Dynamics

The thickness, $b(t)$, of the rim bounding the unsteady expanding sheet is key to the formation of secondary droplets (**Figure 12*c***). This thickness is inherently unsteady, is constantly changing with time, and is set by the balance between incoming fluid from the expanding sheet and the outgoing fluid feeding the ligaments (**Figure 13**). Wang et al. (2018a) showed that the framework of

linear stability analysis cannot capture the evolution of the rim's unsteady thickness. Combining theory with advanced image analysis, Wang et al. (2018a) showed the rim thickness to be governed by an instantaneous local Bond number equal to unity, $Bo(t) = \rho(-\ddot{R}(t))b(t)^2/\sigma = 1$, at all times throughout the extension and retraction of the evolving sheet. Moreover, such a criterion is independent of the impact *We*.

The $Bo(t) = 1$ criterion for the rim dynamics is in fact robust and universal for a family of unsteady inviscid fluid sheet fragmentation phenomena, from impacts of drops on various surface geometries to impacts on films (**Figure 13*a–c***), in a wide range of infectious disease settings (**Figure 2**). Wang et al. (2018a) also showed that the $Bo(t) = 1$ criterion remains valid for a range of viscous and viscoelastic fluids relevant for the unsteady fragmentation of mucosalivary fluids in respiratory disease transmission (Section 3.3). For the same impact *We*, viscous or complex fluids of different viscosity, ν, and elasticity (as measured by the extensional relaxation time, τ_E) maintain the criterion for the rim's local, instantaneous Bond number: $Bo(t) = 1$. For such fluids, the analysis in the local noninertial rim frame gives $\widetilde{Re} = v_b b/\nu$, with $v_b(t) \simeq \sqrt{\sigma/\rho b(t)}$. Likewise, the local Deborah number is $\widetilde{De} = \tau_E/\tau_g$, with $\tau_g \simeq \sqrt{\rho b(t)^3/\sigma}$. The robustness of the $Bo = 1$ criterion continues to hold within the range of $\widetilde{Re} \gtrsim 8$ and $\widetilde{De} \lesssim 16$. Beyond these ranges, additional explicit effects of viscosity or elasticity have to be taken into account.

7.3. Unsteadiness Governs Droplet Sizes and Speeds

Elucidating the dynamics of the unsteady rim allows for closing the coupled system of equations governing the sheet, rim, ligament, and droplets (**Figure 12*c***) and paves the way for predicting the droplet sizes and speeds for such canonical 2D unsteady fragmentation (Wang & Bourouiba 2020a; Y. Wang & L. Bourouiba, manuscripts in review). The unsteadiness of the fragmentation process gives rise to the skewness of the droplet size and speed distributions, although in the local, noninertial reference frame of the moving rim, the distributions are nonskewed. Indeed, Wang & Bourouiba (2018b) recently showed that the instantaneous distributions of droplet size and speed shed throughout the sheet expansion and retraction are symmetric and well approximated by instantaneous Gaussian distributions (**Figure 14*c*,*f***). These instantaneous Gaussian distributions have a mean that evolves with time (**Figure 14*b*,*e***), and the skewness of the reported cumulative distributions (**Figure 14*a*,*d***) is therefore due to the unsteadiness of the sheet expansion and the resulting superposition of (instantaneous) Gaussian distributions with time-varying means. These recent insights are critical for establishing a deterministic unifying framework for the study of unsteady fragmentation, which is at the core of pathogen contaminant and emission, dispersal, persistence, and infection of new hosts in the context of disease transmission (**Figure 1**). This is in contrast to steady fragmentation, where empirical drop size distributions are typically fitted using log-normal, Poisson, exponential, Weibull–Rosin–Rammler, gamma, or compound gamma distributions (Lefebvre & McDonell 2017). These choices all aim to capture the skewness in drop sizes. Some of these distributions, such as the log-normal (sequential breakup) or the gamma [ligament-mediated fragmentation (Villermaux et al. 2004)], are rooted in proposed physical mechanisms governing steady fluid fragmentation, while others are empirical curve fits. Instead, by isolating the effect of the unsteadiness, we can simplify the droplet generation problem to understanding the nonlinear instabilities governing this class of multiscale unsteady fragmentation problems, which have been shown to involve ligament end-pinching, generating one drop at a time (Wang & Bourouiba 2018b). Moreover, the fundamental insights gained have implications for other application domains where unsteady fragmentation is ubiquitous, such as blood stain impact patterns in criminology (Laan et al. 2015), drug delivery, decontamination of produce, and many industrial processes.

8. DISCUSSION AND OUTLOOK

Epidemics, such as 1918 influenza, SARS, or COVID-19, are notoriously difficult to study, in part due to their inherently transient and sudden nature, making it difficult to test hypotheses and determine truly successful mitigation strategies. The transmission phase of infectious diseases, in particular, has largely been a neglected area of research. Hence, in 2020 we find ourselves asking similar questions to those discussed during the 1918 influenza (Soper 1919) and the 2003 SARS pandemics (SARS Comm. 2007, chapter 8), including: What distances of interactions are safe (Jones et al. 2020)? What masks should be used and when (Bahl et al. 2020)? What airflow management ought to be used in indoor spaces? Similarly, we continue to struggle to contain nosocomial infectious agents and have a limited understanding of the flow physics driving a range of crop diseases in fields or food safety postharvest. These gaps may in part be due to a perception of transmission as a highly complex, transient, and essentially stochastic process, suggesting a lack of a mechanistic underpinning. Yet, transmission remains an obligatory step in the life cycle of pathogens; hence, evolutionary pressures would naturally select for robust mechanisms. Indeed, the building block of any epidemic is host-to-host transmission, which, if deciphered, provides an essentially untapped pathway for the development of mitigation and pharmacological and nonpharmacological control innovations (**Figure 1**). Control of smallpox, malaria, or typhoid also seemed obscure and impossible for a long time, yet, in the words of Ross (1910, p. xiii),

> The world requires at least ten years to understand a new idea, however important or simple it may be. The mosquito theorem of malaria was first ridiculed and its application to the saving of human life treated with neglect, jealousy and opposition. But now, owing to the labours of many [...] we are assured of final success.

Ross and his colleagues succeeded in establishing the notion of epidemic reproduction number as a threshold for control of malaria transmission, thus requiring not the impossible task of mosquito eradication, as previously thought, but rather the strategic and threshold-driven management of the mosquito population and its contacts with humans. Advances are possible for mitigation of other infectious diseases, even prior to drug or vaccine development, and start with rigorous quantitative measurements and careful mechanistic understanding of the science of host-to-host transmission, where fluid physics is at the core (**Figure 1**).

The motivation of this review has been to lay out a mechanistic multidisciplinary framework to be leveraged in preparation for and prior to pandemics that are bound to continue to occur, vanish, and return as unexpectedly as they disappeared. This framework breaks down the obligatory transmission phase of a pathogen's life cycle into a rich class of tractable multiscale fluid dynamics problems: the multiphase, particle-laden turbulent nature of exhalations shaping the pathogen footprint of transmission pertinent to respiratory diseases such as COVID-19 or influenza; the complex rheology of fluids and their fragmentation (Sections 3 and 4; Phases 1 and 2 of transmission); the rich coupling between organisms and the fluid phases that shape their dispersal and host-to-host transmission, including the stability of thin films to intrusions, as well as subtle Marangoni flows and their significant effects on the physics and biology of contaminated fluids and on the rich multiscale dynamics of their fragmentation, which shapes indoor contamination risks (Section 5; Phases 1 and 2); the complex fluid–surface interactions entangling compliance, surface wetting, and contaminant–fluid mixing and fragmentation, which are important for not only indoor contamination but also agriculture and food safety applications (Sections 4 and 6; Phases 1 and 2); and the common theme of unsteadiness emerging as central in governing the selection of contamination level, droplet size, and speed distributions via fragmentation, which, when coupled with the local environment in the form of multiphase gas

turbulent clouds or indoor and outdoor environments and the resulting interfacial processes and phase changes, shape the pathogen footprint at the crux of transmission (Section 7). These examples were purposefully drawn from different health application domains to illustrate the full span of scales and rich classes of fluid problems affecting humanity on a daily basis.

An exciting and abundant set of additional questions remain unanswered in each phase of infectious disease transmission and control where fluids and fluid dynamics are at the core. These include the merits of using masks or novel porous materials as source control, the risk of host invasion by droplet nuclei through the conjunctiva, the possible benefits of face shields in addition to face masks, the role of environmental conditions in phase changes indoors and outdoors, and the implications of these conditions for transmission and pathogen persistence. As already mentioned in Section 3.5 in the context of COVID-19, rich fluid dynamic considerations can also inform other infection control and return-to-work strategies, such as the safety of certain medical and patient care procedures or artistic/musical activities involving fluids and respiratory flows; hand washing; adapted social distancing in various confined environments; redesign of indoor confined spaces such as offices, schools, factories, airplanes, or trains; and innovations in surface and air decontamination (air hygiene). Insights can be gained from precise laboratory experiments coupled with modeling to develop and validate specifically tailored solutions for natural or artificial ventilation and indoor air management systems adapted to space usage and occupancy number and duration, where the detailed airflow patterns, rather than the average ventilation, are important for mitigating transmission. Indeed, flow heterogeneities have been implicated in localized clusters of infection, as the well-mixed limit imposed by ventilation is inherently a maximum pathogen dilution limit, thus only providing the lowest possible bound of exposure risk given an indoor space. Fluid-based multiscale modeling of contamination and infection risk can also inform adaptive mitigation strategies and even the development of new drugs that harness critical pathways in fluid-based transmission (Bourouiba 2018). For example, the rheology of a wide range of biological fluids needs further elucidation. Can such fluid properties be manipulated through exogenous additives to reduce a pathogen's affinity for particular fluids to adhere to substrates, whether biological or physical, or to reduce the fluid's ability to disperse the pathogen?

In turn, these exciting applications in health and infectious diseases enable the discovery of new fluid processes and motivate the development of new tools of interest and of broader application beyond the original health domains from which they emerged. For example, fundamental insights gained in unsteady fragmentation were made possible by breakthroughs in image-processing algorithms (works of Y. Wang & L. Bourouiba 2017–2020) and by theory developed for and motivated by the goal of elucidating pathogen transmission. In turn, these breakthroughs have broad industrial and environmental applications. In water-to-air transfer via bubble bursting, organisms were found to manipulate the physics of surface bubbles to enhance their own water-to-air dispersal (Section 5), despite the bacteria's nonmeasurable effect on surface tension, enriching the mysteries of interfacial film dynamics and the ramifications of Marangoni flows. Opportunities exist to develop new analytical, experimental, and numerical tools for interfacial complex, multiphase, and multiscale transient flows to elucidate the important class of emerging problems at the intersection of fluids and health, and beyond.

As this new frontier evolves rapidly, it is ever more important for well-established fluid dynamics methodologies to be further developed and applied, given their successful history of low error tolerance in domains such as aeronautics and astronautics where lives are also at risk. For example, representing human violent exhalations as a hollow vortex ring [as used, e.g., in a recent New York Times simulation (Parshina-Kottas et al. 2020)], rather than a point-source turbulent puff, introduces errors in the range, mixing, and phase change behavior of pathogen-bearing droplets and fails to capture the pathogen footprint underpinning accurate risk assessment.

Frontier high-fidelity numerical tools greatly benefit from validation against high-precision and rigorous experimental data. Quantitative prediction with careful validation will help lay the groundwork for the emerging field of Fluid Dynamics of Disease Transmission and truly impact infectious disease surveillance, control, and prevention, on which lives depend.

Finally, many more exciting mechanisms of interaction between life and physics likely exist in the form of interfacial, multiphase, and complex flows. Their discovery will open new avenues to understanding ecological or evolutionary constraints so far neglected due to the unexplored underlying fluid dynamics governing microorganism dispersal and transmission processes. Understanding such interactions will produce exciting new insights into evolutionary pressures for beneficial, neutral, and pathogenic organisms and, hence, life itself.

DISCLOSURE STATEMENT

The author is not aware of any biases that might be perceived as affecting the objectivity of this review.

ACKNOWLEDGMENTS

The work discussed in this review involved mentoring of and collaborations with students and colleagues with whom it was a pleasure to work, discuss, and exchange over many years. In particular, I would like to thank Donald Aylor, Maria Brandl, John Bush, Nicole Bustos, Lauren Cooper, Eline Dehandschoewercker, Tristan Gilet, James Hughes, Roger Kamm, Sophie Lejeune, Detlef Lohse, Sunny Luo, Claire Lu, Michael Mackey, Taronna Maines, Chiang Mei, Boris Naar, Arne Pearlstein, Stephane Poulain, Kyu Rhee, Barry Scharfman, Alexandra Techet, Emmanuel Villermaux, Yongji Wang, Jianhong Wu, and Stephane Zaleski. The research discussed was supported in part by the MIT Lincoln Laboratory; the USDA–NIFA (US Department of Agriculture–National Institute of Food and Agriculture) Specialty Crop Research Initiative (grant MDW-2016-04938); the MIT Ferry, Reed, and Edgerton Funds; and the Richard and Susan Smith Family Foundation.

LITERATURE CITED

ACS (Am. Cancer Soc.). 2019. *Cancer facts & figures 2019*. Tech. Rep., Am. Cancer Soc., Atlanta, GA. **https://www.cancer.org/research/cancer-facts-statistics/all-cancer-facts-figures/cancer-facts-figures-2019.html**

Agbaglah G, Thoraval MJ, Thoroddsen ST, Zhang LV, Fezzaa K, Deegan RD. 2015. Drop impact into a deep pool: vortex shedding and jet formation. *J. Fluid Mech.* 764:R1

Alsved M, Bourouiba L, Duchaine C, Löndahl J, Marr LC, et al. 2020. Natural sources and experimental generation of bioaerosols: challenges and perspectives. *Aerosol Sci. Technol.* 54:547–71

Atkins KE, Wenzel NS, Ndeffo-Mbah M, Altice FL, Townsend JP, Galvani AP. 2015. Under-reporting and case fatality estimates for emerging epidemics. *BMJ* 350:h1115

Aylor DE. 2017. *Aerial Dispersal of Pollen and Spores*. St. Paul, MN: Am. Phytopathol. Soc.

Bahl P, Doolan C, de Silva C, Chughtai AA, Bourouiba L, MacIntyre CR. 2020. Airborne or droplet precautions for health workers treating coronavirus disease 2019? *J. Infect. Dis.* 2020:jiaa189

Bansil R, Turner BS. 2006. Mucin structure, aggregation, physiological functions and biomedical applications. *Curr. Opin. Colloid Interface Sci.* 11:164–70

Berberović E, Van Hinsberg NP, Jakirlić S, Roisman IV, Tropea C. 2009. Drop impact onto a liquid layer of finite thickness: dynamics of the cavity evolution. *Phys. Rev. E* 79:036306

Best EL, Sandoe JAT, Wilcox MH. 2012. Potential for aerosolization of *Clostridium difficile* after flushing toilets: the role of toilet lids in reducing environmental contamination risk. *J. Hosp. Infect.* 80:1–5

Blanchard D. 1989. The ejection of drops from the sea and with bacteria and their enrichment—a review. *Estuaries* 12:127–37

Blower S. 2004. An attempt at a new analysis of the mortality caused by smallpox and of the advantages of inoculation to prevent it. *Rev. Med. Virol.* 14:275–88

Bolster DT, Linden PF. 2007. Contaminants in ventilated filling boxes. *J. Fluid Mech.* 591:97–116

Boseley S. 2020. Coronavirus 'could infect 60% of global population if unchecked'. *The Guardian*, Feb. 11. **https://www.theguardian.com/world/2020/feb/11/coronavirus-expert-warns-infection-could-reach-60-of-worlds-population**

Bourouiba L. 2013. Understanding the transmission of H5N1. *CAB Rev.* 8:1–8

Bourouiba L. 2016. A sneeze. *N. Engl. J. Med.* 375:e15

Bourouiba L. 2018. *How diseases and epidemics move through a breath of air*. TEDMED Talk, accessed May 16, 2020. **https://www.tedmed.com/talks/show?id=730067**

Bourouiba L. 2020. Turbulent gas clouds and respiratory pathogen emissions: potential implications for reducing transmission of COVID-19. *JAMA* 323:1837–38

Bourouiba L, Bush JWM. 2013. Drops and bubbles in the environment. In *Handbook of Environmental Fluid Dynamics*, Vol. 1: *Overview and Fundamentals*, ed. HJS Fernando, pp. 427–39. Boca Raton, FL: CRC

Bourouiba L, Dehandschoewercker E, Bush JWM. 2014. Violent expiratory events: on coughing and sneezing. *J. Fluid Mech.* 745:537–63

Bourouiba L, Wu J, Newman S, Takekawa J, Natdorj T, et al. 2010. Spatial dynamics of bar-headed geese migration in the context of H5N1. *J. R. Soc. Interface* 7:1627–39

Bremond N, Villermaux E. 2006. Atomization by jet impact. *J. Fluid Mech.* 549:273–306

Bush JWM, Thurber BA, Blanchette FA. 2003. Particle clouds in homogeneous and stratified environments. *J. Fluid Mech.* 489:29–54

CDC (Cent. Dis. Control Prev.). 2017a. *Seasonal flu death estimate increases worldwide*. Press Release, Dec. 13. **https://www.cdc.gov/media/releases/2017/p1213-flu-death-estimate.html**

CDC (Cent. Dis. Control Prev.). 2017b. *Severe acute respiratory syndrome (SARS)*. Web Resour., Cent. Dis. Control Prev., Atlanta, GA, updated Dec. 6. **https://www.cdc.gov/sars/index.html**

CDC (Cent. Dis. Control Prev.). 2019. *Middle east repsiratory syndrome (MERS)—transmission*. Cent. Dis. Control Prev., Atlanta, GA, updated Aug. 2. **http://www.cdc.gov/coronavirus/mers/about/transmission.html**

Clanet C, Villermaux E. 2002. Life of a smooth liquid sheet. *J. Fluid Mech.* 462:307–40

Culick F. 1960. Comments on a ruptured soap film. *J. Appl. Phys.* 31:1128–29

Darlow H, Bale W. 1959. Infective hazards of water-closets. *Lancet* 273:1196–200

Déchelette A, Babinsky E, Sojka PE. 2011. Drop size distributions. In *Handbook of Atomization and Sprays: Theory and Applications*, ed. N Ashgriz, pp. 479–95. Boston: Springer

Ding Z, Qian H, Xu B, Huang Y, Miao T, et al. 2020. Toilets dominate environmental detection of SARS-CoV-2 virus in a hospital. medRxiv 20052175. **https://doi.org/10.1101/2020.04.03.20052175**

Duguid J. 1945. The numbers and the sites of origin of the droplets expelled during expiratory activities. *Edinb. Med. J.* 52:385–401

Duguid J. 1946. The size and the duration of air-carriage of respiratory droplets and droplet-nuclei. *J. Hyg.* 44:471–79

Eggers J, Villermaux E. 2008. Physics of liquid jets. *Rep. Prog. Phys.* 71:036601

Falkinham JO. 2003. Mycobacterial aerosols and respiratory disease. *Emerg. Infect. Dis.* 9:763–67

Fitt B, McCartney H, Walklate P. 1989. The role of rain in dispersal of pathogen inoculum. *Annu. Rev. Phytopathol.* 27:241–70

Flügge C. 1897. Über Luftinfection. *Zeit. Hyg. Infektionskrankh.* 25:179–224

Fones H, Gurr S. 2015. The impact of Septoria tritici Blotch disease on wheat: an EU perspective. *Fungal Genet. Biol.* 79:3–7

Furbish D, Hammer K, Schmeeckle M, Borosund M, Mudd S. 2007. Rain splash of dry sand revealed by high-speed imaging and sticky paper splash targets. *J. Geophys. Res.* 112:F01001

Geagea L, Huber L, Sache I. 1999. Dry-dispersal and rain-splash of brown (*Puccinia recondita* f.sp. *tritci*) and yellow (*P. striiformis*) rust spores from infected wheat leaves exposed to simulated raindrops. *Plant Pathol.* 48:472–82

Gerba CP, Wallis C, Manlike JL. 1975. Microbiological hazards of household toilets: droplet production and the fate of residual organisms. *Appl. Microbiol.* 30:229–37
Gilet T, Bourouiba L. 2014. Rain-induced ejection of pathogens from leaves: revisiting the hypothesis of splash-on-film using high-speed visualization. *Integr. Comp. Biol.* 54:974–84
Gilet T, Bourouiba L. 2015. Fluid fragmentation shapes rain-induced foliar disease transmission. *J. R. Soc. Interface* 12:20141092
Gonnermann HM, Manga M. 2007. The fluid mechanics inside a volcano. *Annu. Rev. Fluid Mech.* 39:321–56
Grotberg JB. 2001. Respiratory fluid mechanics and transport processes. *Annu. Rev. Biomed. Eng.* 3:421–57
Hamner L, Dubbel P, Capron I, Ross A, Jordan A, et al. 2020. High SARS-CoV-2 attack rate following exposure at a choir practice—Skagit County, Washington. *Morb. Mortal. Wkly. Rep.* 69:606–10
Harding L, Campbell D. 2020. Up to 20% of hospital patients with covid-19 caught it at hospital. *The Guardian*, May 17. **https://www.theguardian.com/world/2020/may/17/hospital-patients-england-coronavirus-covid-19**
Hare R. 1964. The transmission of respiratory infections. *Proc. R. Soc. Med.* 57:221–30
Haward S, Odell J, Berry M, Hall T. 2011. Extensional rheology of human saliva. *Rheol. Acta* 50:869–79
Hewitt A. 2000. Spray drift: impact of requirements to protect the environment. *Crop Prot.* 19:623–27
Hirst J. 1995. Bioaerosols: introduction, retrospect and prospect. In *Bioaerosols Handbook*, ed. CS Cox, CM Wathes, pp. 5–14. Boca Raton, FL: CRC
Huber L, Gillespie TJ. 1992. Modeling leaf wetness in relation to plant disease epidemiology. *Annu. Rev. Phytopathol.* 30:553–77
Hunt GR, Linden. 2005. Displacement and mixing ventilation driven by opposing wind and buoyancy. *J. Fluid Mech.* 527:27–55
Hunt JCR, Delfos R, Eames I, Perkins RJ. 2007. Vortices, complex flows and inertial particles. *Flow Turbul. Combust.* 79:207–34
IMF (Int. Monet. Fund)/WB (World Bank). 2006. *Avian flu update*. Press Brief., Sept. 17. **https://www.imf.org/external/mmedia/view.aspx?vid=78598401001**
Johnson DL, Lynch RA, Marshall C, Mead KR, Hirst DV. 2013a. Aerosol generation by modern flush toilets. *Aerosol Sci. Technol.* 47:1047–57
Johnson DL, Mead KR, Lynch RA, Hirst DV. 2013b. Lifting the lid on toilet plume aerosol: a literature review with suggestions for future research. *Am. J. Infect. Control* 41:254–58
Johnson G, Morawska L, Ristovski Z, Hargreaves M, Mengersen K, et al. 2011. Modality of human expired aerosol size distributions. *J. Aerosol Sci.* 42:839–51
Johnston C, Qiu H, Ticehurst J, Dickson C, Rosenbaum P, et al. 2007. Outbreak management and implications of a nosocomial norovirus outbreak. *Clin. Infect. Dis.* 45:534–40
Jones NR, Queshi Z, Temple R, Larwood JPJ, Greenhalgh T, Bourouiba L. 2020. 2 metres or 1? What is the evidence base for physical distancing in the context of COVID-19? *Br. Med. J.* 370:m3223
Josserand C, Thoroddsen ST. 2016. Drop impact on a solid surface. *Annu. Rev. Fluid Mech.* 48:365–91
Josserand C, Zaleski S. 2003. Droplet splashing on a thin liquid film. *Phys. Fluids* 15:1650–57
Jung S, Staples S, Dabiri J, Marsden A, Prakash M, et al. 2016. *Research trends in biological fluid dynamics: a USNCTAM report on recent trends in mechanics*. Tech. Rep., US Natl. Comm. Theor. Appl. Mech., US Natl. Acad. Sci. Eng. Med., Washington, DC
Kesimer M, Makhov AM, Griffith JD, Verdugo P, Sheehan JK. 2010. Unpacking a gel-forming mucin: a view of MUC5B organization after granular release. *Am. J. Physiol. Lung Cell Mol. Physiol.* 289:15–22
Khamsi R. 2020. They say coronavirus isn't airborne—but it's definitely borne by air. *Wired*, Mar. 14. **https://www.wired.com/story/they-say-coronavirus-isnt-airborne-but-its-definitely-borne-by-air/**
Koch R. 1876. Untersuchungen über Bakterien: V. Die Aetiologie der Milzbrandkrankheit, begründet auf der Entwicklungsgeschichte des *Bacillus anthracis*. *Beitr. Biol. Pflanzen* 2:277–310
Kyne L, Hamel H, Polavaram R, Kelly C. 2002. Health care costs and mortality associated with nosocomial diarrhea due to *Clostridium difficile*. *Clin. Infect. Dis.* 42:346–53
Laan N, de Bruin KG, Slenter D, Wilhelm J, Jermy M, Bonn D. 2015. Bloodstain pattern analysis: implementation of a fluid dynamic model for position determination of victims. *Sci. Rep.* 5:11461
Lefebvre AH, McDonell VG. 2017. *Atomization and Sprays*. Boca Raton, FL: CRC. 2nd ed.

Lejeune S, Gilet T, Bourouiba L. 2018. Edge-effect: Liquid sheet and droplets formed by drop impact close to an edge. *Phys. Rev. Fluids* 3:083601

Lessa FC, Mu Y, Bamberg WM, Beldavs ZG, Dumyati GK, et al. 2015. Burden of *Clostridium difficile* infection in the United States. *N. Engl. J. Med.* 372:825–34

Lewis D. 2020. Is the coronavirus airborne? Experts can't agree. *Nature* 580:175

Lhuissier H, Villermaux E. 2012. Bursting bubble aerosols. *J. Fluid Mech.* 696:5–44

Li Y, Qian H, Hang J, Chen X, Hong L, et al. 2020. Evidence for probable aerosol transmission of SARS-CoV-2 in a poorly ventilated restaurant. medRxiv 20067728. **https://doi.org/10.1101/2020.04.16.20067728**

Linden PF. 1999. The fluid mechanics of natural ventilation. *Annu. Rev. Fluid Mech.* 31:201–38

Liu Y, Ning Z, Chen Y, Guo M, Liu Y, et al. 2020. Aerodynamic analysis of SARS-CoV-2 in two Wuhan hospitals. *Nature* 582:557–60

Lohse D, Zhang X. 2020. Physicochemical hydrodynamics of droplets out of equilibrium: a perspective review. arXiv:2005.03782 [physics.flu-dyn]

Madden LV, Hughes G, van den Bosch F. 2007. *The Study of Plant Disease Epidemics*. St. Paul, MN: Am. Phytopathol. Soc. 2nd ed.

Majumder MS, Brownstein JS, Finkelstein SN, Larson RC, Bourouiba L. 2017. Nosocomial amplification of MERS-coronavirus in South Korea, 2015. *Trans. R. Soc. Trop. Med. Hyg.* 111:261–69

Martin D, Nokes R. 1988. Crystal settling in a vigorously convecting magma chamber. *Nature* 332:534–36

Maxworthy T. 1972. The structure and stability of vortex rings. *J. Fluid Mech.* 51:15–32

Mbareche H, Veillette M, Teertstra W, Kegel W, Bilodeau GJ, et al. 2019. Recovery of fungal cells from air samples: a tale of loss and gain. *Appl. Environ. Microbiol.* 85:e02941-18

Mead PS, Slutsker L, Dietz V, McCaig LF, Bresee JS, et al. 1999. Food-related illness and death in the United States. *Emerg. Infect. Dis.* 5:607–25

Meredith D. 1973. Significance of spore release and dispersal mechanisms in plant disease epidemiology. *Annu. Rev. Phytopathol.* 11:313–42

Mokyr J. 2020. Great famine. *Encyclopædia Britannica*, updated Feb. 4. **https://www.britannica.com/event/Great-Famine-Irish-history**

Morawska L, Johnson GR, Ristovski ZD, Hargreaves M, Mengersen K, et al. 2009. Size distribution and sites of origin of droplets expelled from the human respiratory tract during expiratory activities. *J. Aerosol Sci.* 40:256–69

Morton BR, Taylor GI, Turner JS. 1956. Turbulent gravitational convection from maintained and instantaneous sources. *Proc. R. Soc. A* 234:1–23

Néel B, Villermaux E. 2018. The spontaneous puncture of thick liquid films. *J. Fluid Mech.* 838:192–221

Nelson KE, Williams CM. 2014. *Infectious Disease Epidemiology: Theory and Practice*. Burlington, MA: Jones & Bartlett. 3rd ed.

Ong SWX, Tan YK, Chia PY, Lee TH, Ng OT, et al. 2020. Air, surface environmental, and personal protective equipment contamination by severe acute respiratory syndrome coronavirus 2 (SARS-CoV-2) from a symptomatic patient. *JAMA* 323:1610–12

Ouyang W, Han J. 2019. Universal amplification-free molecular diagnostics by billion-fold hierarchical nanofluidic concentration. *PNAS* 116:16240–49

Papineni RS, Rosenthal FS. 2009. The size distribution of droplets in the exhaled breath of healthy human subjects. *J. Aerosol Med.* 10:105–16

Park RF. 2007. Stem rust of wheat in Australia. *Aust. J. Agric. Res.* 58:558–66

Parshina-Kottas Y, Saget B, Patanjali K, Fleisher O, Gianordol G. 2020. This 3-D simulation shows why social distancing is so important. *New York Times*, April 14. **https://www.nytimes.com/interactive/2020/04/14/science/coronavirus-transmission-cough-6-feet-ar-ul.html**

Pasteur L. 1861. Memoire sur les corpuscules organisés qui existent dans l'atmosphère; examen de la doctrine de générations spontanées. *Ann. Sci. Nat.* 16:5–98

Paul P, El-Allaf S, Lipps P, Madden L. 2004. Rain splash dispersal of *Gibberella zeae* within wheat canopies in Ohio. *Phytopathol.* 94:1342–49

Poulain S, Bourouiba L. 2018. Biosurfactants change the thinning of contaminated bubbles at bacteria-laden water interfaces. *Phys. Rev. Lett.* 121:204502

Poulain S, Bourouiba L. 2019. Disease transmission via drops and bubbles. *Phys. Today* 72:70
Poulain S, Villermaux E, Bourouiba L. 2018. Aging and burst of surface bubbles. *J. Fluid Mech.* 851:636–71
Prussin AJ, Schwake DO, Marr LC. 2017. Ten questions concerning the aerosolization and transmission of *Legionella* in the built environment. *Build. Environ.* 123:684–95
Reynolds K, Madden L, Reichard D, Ellis M. 1987. Methods for study of raindrop impact on plant surfaces with application to predicting inoculum dispersal by rain. *Phytopathology* 77:226–32
Roisman IV, Prunet-Foch B, Tropea C, Vignes-Adler M. 2002. Multiple drop impact onto a dry solid substrate. *J. Colloid Interface Sci.* 256:396–410
Roisman IV, Tropea C. 2002. Impact of a drop onto a wetted wall: description of crown formation and propagation. *J. Fluid Mech.* 472:373–97
Römkens M, Helming K, Prasad S. 2002. Soil erosion under different rainfall intensities, surface roughness, and soil water regimes. *CATENA* 46:103–23
Roper M, Seminara A. 2019. Mycofluidics: the fluid mechanics of fungal adaptation. *Annu. Rev. Fluid Mech.* 51:511–38
Ross RD. 1910. *The Prevention of Malaria*. New York: E.P. Dutton & Co.
Rozhkov A, Prunet-Foch B, Vignes-Adler M. 2004. Dynamics of a liquid lamella resulting from the impact of a water drop on a small target. *Proc. R. Soc. A* 460:2681–704
Ruhl CR, Pasko BL, Khan HS, Kindt LM, Stamm CE, et al. 2020. *Mycobacterium tuberculosis* sulfolipid-1 activates nociceptive neurons and induces cough. *Cell* 181:293–305.e11
SARS Comm. 2007. *The SARS Commission Final Report*, Vol. 3: *Spring of Fear*. Toronto: Comm. Investig. Intro. Spread SARS Ontario
Scharfman BE, Techet AH, Bush JWM, Bourouiba L. 2016. Visualization of sneeze ejecta: steps of fluid fragmentation leading to respiratory droplets. *Exp. Fluids* 57:24
Scorer RS. 1978. *Environmental Aerodynamics*. West Sussex, UK: Ellis Horwood
Shrestha SS, Swerdlow DL, Borse RH, Prabhu VS, Finelli L, et al. 2011. Estimating the burden of 2009 pandemic influenza A (H1N1) in the United States (April 2009–April 2010). *Clin. Infect. Dis.* 52:75–82
Siegel J, Rhinehart E, Jackson M, Chiarello L. 2007. *2007 guideline for isolation precautions: preventing transmission of infectious agents in healthcare settings*. Healthc. Guidel., Cent. Dis. Control Prev., Atlanta, GA, updated July 2019. **https://www.cdc.gov/infectioncontrol/guidelines/isolation/index.html**
Socolofsky SA, Crounse BC, Adams EE. 2002. Multi-phase plumes in uniform, stratified, and flowing environments. In *Environmental Fluid Mechanics: Theories and Applications*, ed. HH Shen, AHD Cheng, K-H Wang, MH Teng, CCK Liu, pp. 85–125. Reston, VA: Am. Soc. Civil Eng.
Sonkin LS. 1951. The role of particle size in experimental airborne infection. *Am. J. Hyg.* 53:337–54
Soper G. 1919. The lessons learned from the pandemic. *Science* 49:501–6
Strange R, Scott P. 2005. Plant disease: a threat to global food security. *Annu. Rev. Phytopathol.* 43:83–116
Straub H. 1970. Bernoulli, Daniel. In *Dictionary of Scientific Biography, American Council of Learned Societies*, Vol. 2, ed. C Gillespie, pp. 36. New York: Scribner
Su J. 2018. *Biological and particulate contaminants in interfaces*. Master's Thesis, MIT, Cambridge, MA
Taylor GI. 1959. The dynamics of thin sheets of fluid. III. Disintegration of fluid sheets. *Proc. R. Soc. A* 253:313–21
Traverso G, Laken S, Lu CC, Maa R, Langer R, Bourouiba L. 2013. Fluid fragmentation from hospital toilets. arXiv:1310.5511 [physics.flu-dyn]
Turner JS. 1979. *Buoyancy Effects in Fluids*. Cambridge, UK: Cambridge Univ. Press
Vauquelin O. 2015. Oscillatory behaviour in an emptying–filling box. *J. Fluid Mech.* 781:712–26
van Doremalen N, Bushmaker T, Morris DH, Holbrook MG, Gamble A, et al. 2020. Aerosol and surface stability of SARS-COV-2 as compared with SARS-COV-1. *N. Engl. J. Med.* 382:1564–67
Vernay C, Ramos L, Ligoure C. 2015. Free radially expanding liquid sheet in air: time- and space-resolved measurement of the thickness field. *J. Fluid Mech.* 764:428–44
Veron F. 2015. Ocean spray. *Annu. Rev. Fluid Mech.* 47:507–38
Villermaux E. 2007. Fragmentation. *Annu. Rev. Fluid Mech.* 39:419–46
Villermaux E, Bossa B. 2011. Drop fragmentation on impact. *J. Fluid Mech.* 668:412–35
Villermaux E, Marmottant P, Duplat J. 2004. Ligament-mediated spray formation. *Phys. Rev. Lett.* 92:074501

Walls PLL, Bird JC, Bourouiba L. 2014. Moving with bubbles: a review of the interactions between bubbles and the microorganisms that surround them. *Integr. Comp. Biol.* 54:1014–25
Wang D, Hu B, Hu C, Zhu F, Liu X, et al. 2020. Clinical characteristics of 138 hospitalized patients with 2019 novel coronavirus–infected pneumonia in Wuhan, China. *JAMA* 323:1061–69
Wang Y, Bourouiba L. 2017. Drop impact on small surfaces: thickness and velocity profiles of the expanding sheet in the air. *J. Fluid Mech.* 814:510–34
Wang Y, Bourouiba L. 2018a. Non-isolated drop impact on surfaces. *J. Fluid Mech.* 835:24–44
Wang Y, Bourouiba L. 2018b. Unsteady sheet fragmentation: droplet sizes and speeds. *J. Fluid Mech.* 848:946–67
Wang Y, Bourouiba L. 2020a. Growth and breakup of ligaments in unsteady fragmentation. *J. Fluid Mech.* In press
Wang Y, Bourouiba L. 2020b. Non-Galilean Taylor–Culick's law governs sheet dynamics in unsteady fragmentation. *J. Fluid Mech.* In press
Wang Y, Dandekar R, Bustos N, Poulain S, Bourouiba L. 2018a. Universal rim thickness in unsteady sheet fragmentation. *Phys. Rev. Lett.* 120:204503
Wang Y, You W, Fan J, Jin M, Wei X, Wang Q. 2018b. Effects of subsequent rainfall events with different intensities on runoff and erosion in a coarse soil. *CATENA* 170:100–7
Wei W, Jia F, Yang L, Chen L, Zhang H, Yu Y. 2014. Effects of surficial condition and rainfall intensity on runoff in a loess hilly area, China. *J. Hydrol.* 513:115–26
Wells WF. 1934. On air-born infection. Study II. Droplet and droplet nuclei. *Am. J. Epidemiol.* 20:611–18
Wells WF. 1955. *Airborne Contagion and Air Hygiene: An Ecological Study of Droplet Infection*. Cambridge, MA: Harvard Univ. Press
WHO (World Health Org.). 2014. Ebola Response Team Ebola virus disease in West Africa—the first 9 months of the epidemic and forward projections. *N. Engl. J. Med.* 371:1481–95
WHO (World Health Org.). 2018. *Global Health Observatory (GHO) data: tuberculosis (TB)*. Fact Sheet, World Health Org., Geneva, accessed April 6. **https://www.who.int/gho/tb/en/**
Woods AW. 2010. Turbulent plumes in nature. *Annu. Rev. Fluid Mech.* 42:391–412
Yang S, Lee GWM, Chen CM, Wu CC, Yu KP. 2007. The size and concentration of droplets generated by coughing in human subjects. *J. Aerosol Med.* 20:484–94
Yarin AL. 2006. Drop impact dynamics: splashing, spreading, receding, bouncing.... *Annu. Rev. Fluid Mech.* 38:159–92
Zanin M, Baviskar P, Webster R, Webby R. 2016. The interaction between respiratory pathogens and mucus. *Cell Host Microbe* 19:159–68
Zayas G, Chiang M, Wong E, MacDonald F, Lange C, et al. 2012. Cough aerosol in healthy participants: fundamental knowledge to optimize droplet-spread infectious respiratory disease management. *BMC Pulm. Med.* 12:11
Zhang LV, Toole J, Fezzaa K, Deegan RD. 2012. Splashing from drop impact into a deep pool: multiplicity of jets and the failure of conventional scaling. *J. Fluid Mech.* 703:402–13

Annual Review of Fluid Mechanics

Volume 53, 2021

Contents

Indexes

Errata

An online log of corrections to *Annual Review of Fluid Mechanics* articles may be found at http://www.annualreviews.org/errata/fluid